Resource

Cell Stem Cell

Distinct Imprinting Signatures and Biased Differentiation of Human Androgenetic and Parthenogenetic Embryonic Stem Cells

Graphical Abstract

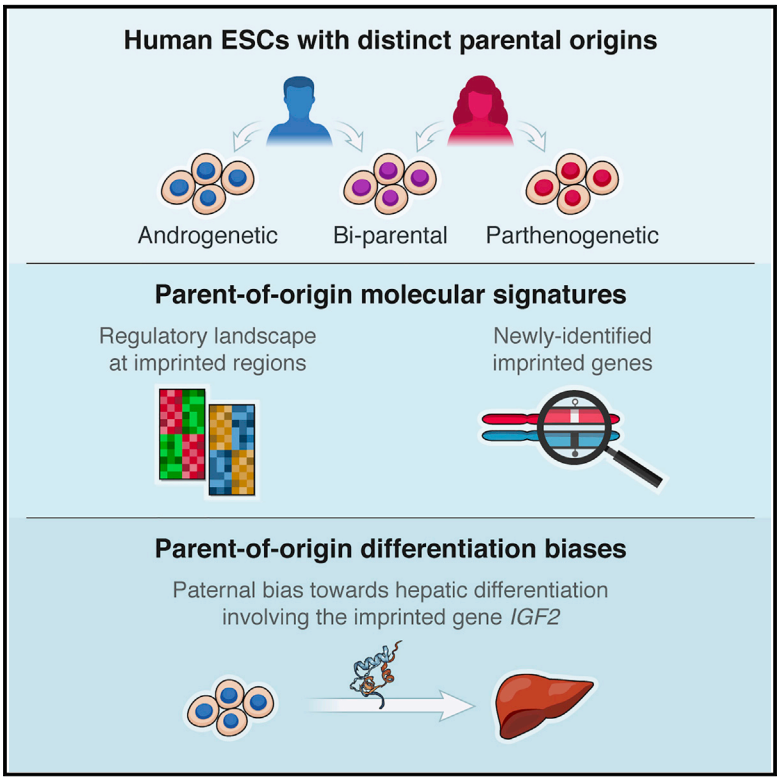

Highlights

- Generation of human androgenetic and parthenogenetic ESCs (aESCs and pESCs)
- Comparing aESCs and pESCs identifies known and formerly undescribed imprinted genes
- The uniparental cells show tissue-specific parent-of-origin differentiation biases
- The imprinted gene *IGF2* is involved in hepatic differentiation bias of human aESCs

Authors

Ido Sagi, Joao C. De Pinho, Michael V. Zuccaro, ..., Rogerio Lobo, Nissim Benvenisty, Dieter Egli

Correspondence

nissimb@mail.huji.ac.il (N.B.), de2220@cumc.columbia.edu (D.E.)

In Brief

Benvenisty, Egli, and colleagues combine newly derived human androgenetic ESCs with parthenogenetic and bi-parental ESCs to explore parental imprinting in humans, charting the regulatory landscape of known imprinted loci, identifying previously undescribed imprinted genes, and interrogating the nature and mechanisms underlying parental-origin-driven tissue-specific differentiation biases with implications for human development and disease.

Sagi et al., 2019, Cell Stem Cell *25*, 419–432
September 5, 2019
https://doi.org/10.1016/j.stem.2019.06.013

CellPress

Cell Stem Cell
Resource

Distinct Imprinting Signatures and Biased Differentiation of Human Androgenetic and Parthenogenetic Embryonic Stem Cells

Ido Sagi,[1] Joao C. De Pinho,[2] Michael V. Zuccaro,[3] Chen Atzmon,[1] Tamar Golan-Lev,[1] Ofra Yanuka,[1] Robert Prosser,[2] Alexandra Sadowy,[2] Gloria Perez,[4] Thiago Cabral,[5] Benjamin Glaser,[6] Stephen H. Tsang,[5] Robin Goland,[7] Mark V. Sauer,[2,8] Rogerio Lobo,[2] Nissim Benvenisty,[1,9,*] and Dieter Egli[2,7,*]

[1]The Azrieli Center for Stem Cells and Genetic Research, Department of Genetics, Silberman Institute of Life Sciences, The Hebrew University, Jerusalem 91904, Israel
[2]Department of Obstetrics and Gynecology and Columbia University Fertility Center, Columbia University, College of Physicians & Surgeons, New York, NY 10032, USA
[3]Department of Cellular Physiology and Biophysics, Columbia University, New York, NY 10032, USA
[4]The New York Stem Cell Foundation Research Institute, New York, NY 10019, USA
[5]Departments of Ophthalmology and Pathology and Cell Biology, Columbia Stem Cell Initiative, Columbia University, New York, NY 10032, USA
[6]Hadassah Medical Center, Department of Endocrinology, Jerusalem 9112001, Israel
[7]Department of Pediatrics, Naomi Berrie Diabetes Center, Columbia Stem Cell Initiative, Columbia University, New York, NY 10032, USA
[8]Present address: Robert Wood Johnson Medical School, Rutgers University, New Brunswick, NJ 08854, USA
[9]Lead Contact
*Correspondence: nissimb@mail.huji.ac.il (N.B.), de2220@cumc.columbia.edu (D.E.)
https://doi.org/10.1016/j.stem.2019.06.013

SUMMARY

Genomic imprinting is an epigenetic mechanism that results in parent-of-origin monoallelic expression of specific genes, which precludes uniparental development and underlies various diseases. Here, we explored molecular and developmental aspects of imprinting in humans by generating exclusively paternal human androgenetic embryonic stem cells (aESCs) and comparing them with exclusively maternal parthenogenetic ESCs (pESCs) and bi-parental ESCs, establishing a pluripotent cell system of distinct parental backgrounds. Analyzing the transcriptomes and methylomes of human aESCs, pESCs, and bi-parental ESCs enabled the characterization of regulatory relations at known imprinted regions and uncovered imprinted gene candidates within and outside known imprinted regions. Investigating the consequences of uniparental differentiation, we showed the known paternal-genome preference for placental contribution, revealed a similar bias toward liver differentiation, and implicated the involvement of the imprinted gene *IGF2* in this process. Our results demonstrate the utility of parent-specific human ESCs for dissecting the role of imprinting in human development and disease.

INTRODUCTION

In mammals, the maternal and paternal genomes that unite at fertilization to form the next generation are functionally non-equivalent due to genomic imprinting, an epigenetic mechanism that results in parent-of-origin monoallelic expression of a specific subset of genes (Barlow and Bartolomei, 2014; Reik and Walter, 2001). Imprinted gene expression is regulated by parent-of-origin-dependent DNA methylation acquired differentially at specific genomic loci during gametogenesis and maintained throughout development and adult life. Germline differentially methylated regions (DMRs) serve as control elements that instruct additional epigenetic changes in *cis*, including the establishment of secondary DMRs during development and, most notably, the parent-specific regulation of adjacent imprinted genes by various mechanisms (Lee and Bartolomei, 2013). Because imprinted genes are preferentially expressed from one of the parental alleles, genomic contributions from both parents are required for proper embryogenesis (McGrath and Solter, 1984; Surani and Barton, 1983; Surani et al., 1984). Moreover, as imprinted genes are involved in diverse physiological processes, their dysregulation is associated with a variety of human diseases ranging from developmental syndromes to metabolic and neurological disorders to cancer (Peters, 2014).

Key advances in imprinting research have emerged from the use of uniparental cells, which enable systematic dissection of parent-of-origin effects in isolated parental backgrounds at the molecular and functional levels. Exclusively maternal cells can arise by parthenogenesis or gynogenesis, which involve activation of an unfertilized oocyte or loss of the paternal genome after fertilization, respectively. Complementarily, exclusively paternal cells can be produced by androgenesis, whereby paternal genome(s) are introduced into an oocyte whose own genome is lost or discarded. Although imprinting precludes uniparental development after implantation (McGrath and Solter, 1984; Surani and Barton, 1983; Surani et al., 1984), uniparental mouse embryos can form blastocysts and give rise to embryonic stem cells (ESCs) of either parthenogenetic (pESCs) or androgenetic origin (aESCs) (Kaufman et al., 1983; Mann et al., 1990). Later, similar techniques have been employed to generate human pESCs

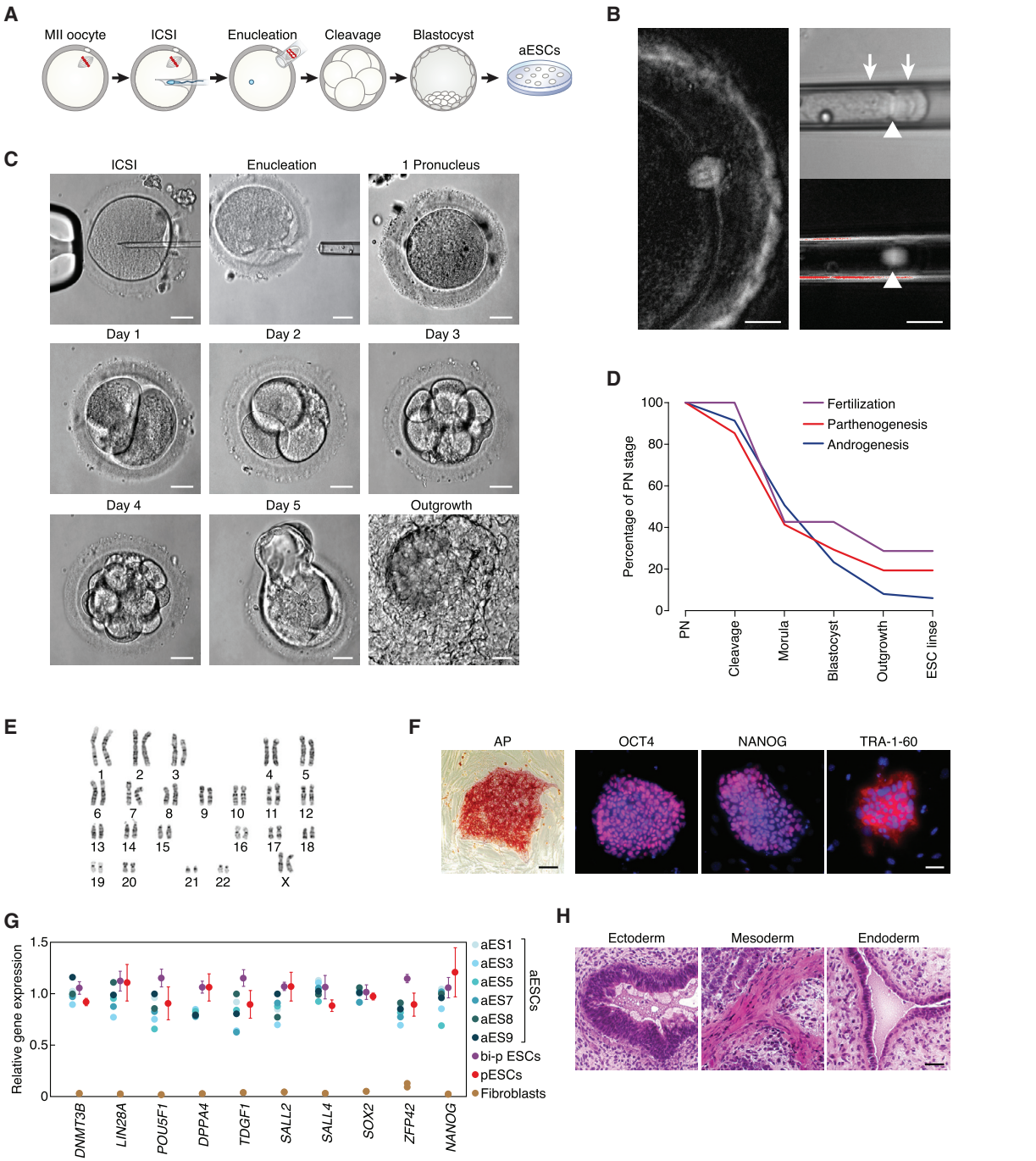

Figure 1. Derivation of Human aESC Lines

(A) Experimental scheme for the derivation of human aESCs following ICSI into MII oocytes and oocyte enucleation.

(B) Removal of the maternal genome in anaphase II. Left image shows the anaphase II oocyte 3 h after ICSI. Right images show the removed spindle-chromosome complex in the pipette in bright field (top) and by microtubule birefringence (bottom). Arrows point to the maternal genomes directed toward the forming polar body (right arrow) and the oocyte (left arrow). Arrowhead points to the abscission point. Scale bar, 20 μm.

(C) Representative images of the developmental stages of *in vitro* androgenesis. Scale bar, 20 μm.

(D) Developmental efficiency during *in vitro* fertilization, parthenogenesis, and androgenesis, shown as the percentage of embryos reaching each stage relative to the total number of pronuclear (PN) stage oocytes.

(E) 46,XX karyotype of human aESCs (aES1).

(legend continued on next page)

(Kim et al., 2007b; Revazova et al., 2007), and, more recently, a single human aESC line has been reported as well (Ding et al., 2015).

Despite the competence of uniparental ESCs to differentiate de facto into cells of the three embryonic germ layers (Ding et al., 2015; Kaufman et al., 1983; Kim et al., 2007b; Revazova et al., 2007; Teramura et al., 2009), in developmental contexts, uniparental cells and embryos show severely abnormal phenotypes and biased contributions toward certain lineages. In mice, parthenogenetic and gynogenetic conceptuses arrest by mid-gestation, comprising an embryo proper with poorly developed extraembryonic tissues, whereas androgenetic conceptuses fail earlier, consisting predominantly of extraembryonic trophoblast and an aberrantly developed embryo (Barton et al., 1984; Kaufman et al., 1977; McGrath and Solter, 1984; Surani and Barton, 1983; Surani et al., 1984, 1986). Similarly, natural parthenogenesis in women results in ovarian teratomas composed of diverse embryonic tissues, whereas androgenesis generates trophoblastic tumors known as hydatidiform moles (Kajii and Ohama, 1977; Linder et al., 1975). These reciprocal phenotypes suggest that the maternal and paternal genomes provide complementary contributions with respect to embryonic and extraembryonic development. Nevertheless, subsequent studies on mouse chimeric embryos combining uniparental and bi-parental cells also revealed differential spatial distributions of androgenetic and parthenogenetic cells across body tissues, implying that each parental genome also features different capacities and deficiencies in differentiation into specific embryonic lineages (Barton et al., 1991; Fundele et al., 1989, 1990; Mann et al., 1990; Nagy et al., 1989).

Although imprinting is conserved between mouse and human, the vast majority of annotated imprinted genes are not shared between the species (Tucci et al., 2019), suggesting that species-specific imprinting patterns likely exert unique effects on human development and disease. To investigate both molecular and developmental aspects of imprinting in humans, we established a pluripotent cell system of human ESC lines with distinct parental origins, comprising newly derived all-paternal aESCs, all-maternal pESCs, and related bi-parental ESCs. The characteristic transcriptional and epigenetic imprinting signatures of these cells enabled us to analyze regulatory relations at known imprinted loci, as well as to identify previously undescribed imprinted gene candidates. Furthermore, we utilized the pluripotency of our system to perform a developmental study of human uniparental cells, uncovering tissue-specific parent-of-origin biases with potential implication for human development and disease.

RESULTS

The Maternal Spindle Augments Oocyte Activation

To derive human aESC lines, we developed a modified nuclear transfer technique based on intracytoplasmic sperm injection (ICSI) followed by oocyte enucleation (see STAR Methods). A total of 155 oocytes from 15 different donors were used, of which 136 were freshly obtained and 19 were cryopreserved (22 oocytes lysed during thawing, enucleation or ICSI). Sperm from four different donors were used. In initial experiments, 17 oocytes in metaphase II (MII) were enucleated prior to ICSI, resulting in 10 oocytes (59%) with a single pronucleus (Table S1). None of these developed to the blastocyst stage, suggesting that the sperm alone was inefficient in activating the oocyte in the absence of the maternal spindle. To facilitate oocyte activation, we added puromycin for 3 h after ICSI into enucleated oocytes. Puromycin inhibits translation and thereby mediates oocyte activation (Yamada et al., 2014). Of 14 oocytes, 12 (86%) formed one-pronuclear zygotes. To directly determine whether the presence of the oocyte spindle during anaphase facilitates oocyte activation and androgenetic development, we performed ICSI into MII oocytes and enucleated them at anaphase II 3 h after injection (Figures 1A and 1B). Of 95 injected oocytes, 81 (85%) formed a single pronucleus (Table S1). Fertilization rates of around 80% are normal after ICSI (Palermo et al., 2009). Therefore, the presence of the maternal spindle during meiosis II facilitates oocyte activation. This may involve Aurora-B kinase, which localizes to the midbody during chromosome segregation, thereby segregating the kinase from the histones it phosphorylates, promoting chromosome condensation (Goto et al., 2002). This relocalization to the midbody cannot occur in the absence of a spindle.

Preimplantation Development of Androgenotes

Of the oocytes subjected to ICSI, seven were fertilized without enucleation (*in vitro* fertilization, IVF), and 43 additional oocytes were activated by parthenogenesis (Table S1). Androgenesis, parthenogenesis, and IVF all yielded blastocyst stage embryos (Figures 1C and 1D). Notably, arrest at the cleavage stage was common in all procedures, and the percentage of cleavage-arrested androgenetic embryos (50%) was not elevated compared with parthenogenetic and IVF controls (Figure 1D). However, 27% of androgenotes arrested at the morula stage, and only 23% formed blastocysts, compared with 43% in IVF controls and 29% in parthenotes (Figure 1D). Gametes from all four sperm donors gave rise to androgenetic blastocysts. Considering that half of the resulting androgenetic embryos should be non-viable for lacking an X chromosome (originating from a Y chromosome carrying sperm), the developmental success rate of human androgenotes was comparable to that of IVF embryos.

Derivation of Pluripotent Human aESC Lines

Of 23 blastocysts generated by ICSI followed by oocyte enucleation, we obtained eight ESC outgrowths (35%), and, of these, six human aESC lines were derived (Table S1), as also confirmed by their homozygosity and genetic match to sperm donors based on short tandem repeat (STR) analysis (Table S2). Two outgrowths, both from the same sperm donor, were lost for technical reasons during early passaging. aES1 and aES3 originated

(F) Alkaline phosphatase (AP) staining (left panel) and immunofluorescence staining of pluripotency markers OCT4, NANOG, and TRA-1-60 (red) and DNA (blue, right panel) in human aESC colonies (aES1). Scale bar, 50 μm.

(G) Expression levels of pluripotent stem cell specific genes in human aESCs (n = 6), pESCs (n = 5, mean ± SEM), bi-parental (bi-p) ESCs (n = 8, mean ± SEM), and fibroblasts (n = 2) relative to the median in bi-parental ESCs (replicates detailed in Table S4).

(H) Representative histological sections of an aES1-derived teratoma, demonstrating differentiation into the three embryonic germ layers. Scale bar, 50 μm.

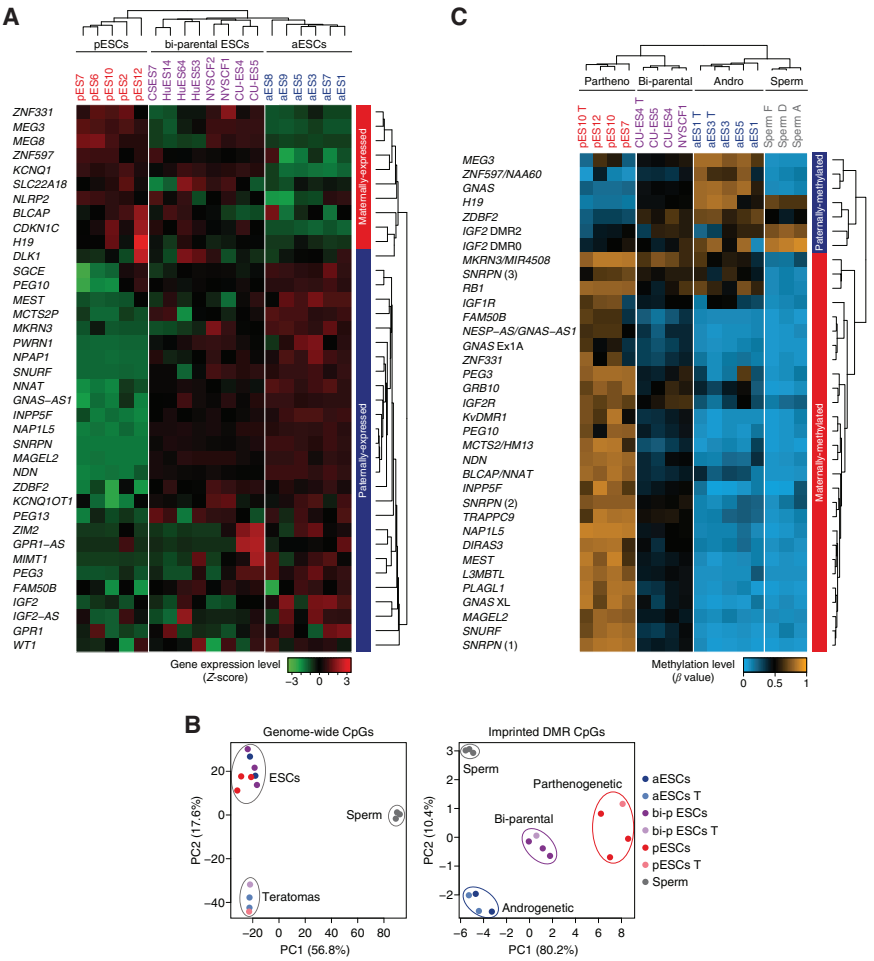

Figure 2. Imprinting Status of Known Imprinted Loci in Human aESCs

(A) Expression levels of known imprinted genes in human aESCs, pESCs, and bi-parental ESCs (replicates detailed in Table S4).

(B) PCA of DNA methylation levels at genome-wide CpGs (left panel) and CpGs within known imprinted DMRs (right panel) in undifferentiated human aESCs, pESCs, and bi-parental (bi-p) ESCs, as well as teratomas (T) generated from these cells and sperm samples. Percentages of explained variation are indicated in parentheses (replicates detailed in Table S5).

(C) DNA methylation levels at known imprinted DMRs in undifferentiated human aESCs, pESCs, and bi-parental ESCs, as well as teratomas (T) generated from these cells and sperm samples. Andro, androgenetic; partheno, parthenogenetic (replicates detailed in Table S5).

from one sperm donor (genetically distinct at 50% of 10 polymorphic STRs), aES5 was derived from a second donor, and aES7, aES8, and aES9 resulted from a third donor (genetically distinct at 64% of 11 polymorphic STRs on average) (Table S2). All aESC lines had a diploid female karyotype (Figures 1E and S1). The homozygous diploid nature of early-passage aESCs indicated rapid diploidization of haploid androgenetic cells, as previously observed in the derivation of pESCs (Sagi et al., 2016a).

Furthermore, from the three blastocysts derived after ICSI without enucleation, we derived two diploid, female bi-parental cell lines (CU-ES4 and CU-ES5) (Figure S1), which are paternally related to aESC lines aES1 and aES3. In addition, from 12 parthenogenetic blastocysts, we derived eight pESC lines. Together, ESC derivation efficiency was significantly lower after androgenesis (6 aESC lines of 81 pronuclear stage oocytes, 7.4%) than after either parthenogenesis (8/41, 20%) or bi-parental development (2/7, 29%). The generation of Y-only embryos is a likely reason for the reduced efficiency, though donor-specific differences in the ability to establish ESC lines cannot be excluded.

Human aESCs exhibited the classic characteristics of pluripotent cells, including self-renewal, colony morphology, alkaline phosphatase activity, expression of specific cell-surface markers, and expression of pluripotency-related genes at comparable levels to those observed in bi-parental ESCs and pESCs (Figures 1F and 1G). Upon injection into immunodeficient mice, human aESCs formed teratomas comprising differentiated cells representing the three embryonic germ layers (Figure 1H), consistent with previous findings in mouse aESCs and a single human aESC line (Ding et al., 2015; Teramura et al., 2009).

Human aESCs Feature Genome-wide Paternal Imprinting

As the genome of human aESCs is exclusively sperm derived, these cells should exhibit genome-wide transcriptional and epigenetic signatures of paternal imprinting. To assess the global imprinting status, we first compared the expression levels of genes that are known to be imprinted in humans by performing RNA sequencing (RNA-seq) in human aESCs, pESCs, and bi-parental ESCs (Table S3; see STAR Methods). The different ESC lines clustered by parental origin, and, relative to bi-parental ESCs, maternally expressed genes (MEGs) were generally downregulated in aESCs and upregulated in pESCs, whereas paternally expressed genes (PEGs) showed the opposite trend (Figure 2A). We have previously shown that imprinted genes overlapping non-imprinted transcripts or having tissue-specific expression are difficult to detect by conventional transcriptome analyses (Stelzer et al., 2015). However, several such genes (*MEST*, *INPP5F*, *IGF2*, *KCNQ1*, *WT1*, *PWRN1*, *ZIM2*, *PEG3*, *BLCAP*, and *GNAS-AS1*) did show parent-specific differential expression (Figure 2A). Moreover, a few genes with only provisional evidence for imprinting (*GPR1*, *PEG13*, *SLC22A18*, *ZNF331*, and *NLRP2*) also displayed this expression pattern, providing additional support for their imprinted status (Figure 2A).

We next analyzed DNA methylation levels within known imprinted DMRs in human aESCs, pESCs, and bi-parental ESCs, as well as teratomas derived from these cells and donor sperm samples by methylation profiling arrays (Table S3; see STAR Methods). By principal-component analysis

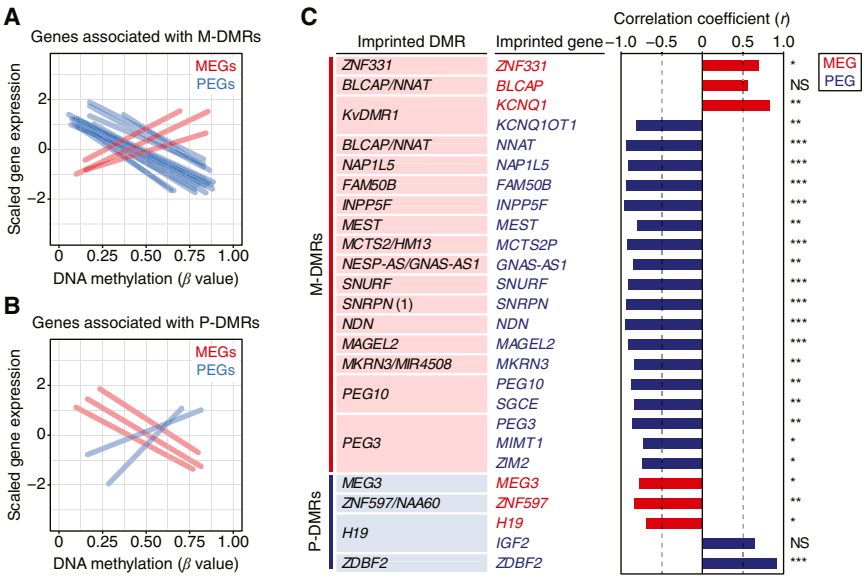

Figure 3. Correlation between Imprinted Gene Expression and DNA Methylation at Corresponding DMRs

(A and B) Linear regression analysis of imprinted gene expression and DNA methylation levels at associated M-DMRs (A) and P-DMRs (B) (see Figure S3). Red and blue curves denote MEGs and PEGs, respectively.

(C) Correlation coefficients of gene expression and DNA methylation levels for individual imprinted genes and corresponding DMRs. *p < 0.05, **p < 0.01, ***p < 0.001. NS, non-significant (linear regression).

(PCA) of genome-wide DNA methylation, aESCs clustered with bi-parental ESCs and pESCs and apart from sperm samples and teratomas derived from these cells (Figure 2B). However, differential DNA methylation levels specifically at imprinted DMRs resulted in distinct segregation of different samples by parental origin rather than by cell type (Figure 2B), consistent with the maintenance of imprinted methylation during differentiation.

Bi-parental samples showed intermediate DNA methylation levels across imprinted DMRs, reflecting a composite of hypomethylated and hypermethylated alleles (Figure 2C). As expected, maternally methylated DMRs (M-DMRs) were hypomethylated in sperm, predominantly hypomethylated in androgenetic cells and hypermethylated in parthenogenetic cells. In contrast, paternally methylated DMRs (P-DMRs) were hypermethylated in androgenetic cells and predominantly hypomethylated in parthenogenetic cells. Importantly, analysis of P-DMRs revealed not only sperm-methylated germline DMRs (*H19*, *IGF2*, and *ZDBF2*) but also secondary DMRs (*MEG3*, *ZNF597/NAA60*, and *GNAS*), which are unmethylated in sperm but gained paternal-specific methylation during the development of early androgenetic embryos and aESCs. Notably, DNA methylation at the sperm-methylated region of the *ZDBF2* DMR expanded in androgenetic and bi-parental ESCs and teratomas, but not in parthenogenetic samples, as observed across normal bi-parental tissues (Figure S2A). Differential DNA methylation of this DMR in aESCs and pESCs was further confirmed by bisulfite sequencing (Figure S2B).

Gene Expression Correlates with DNA Methylation at Imprinted Loci

The collection of human ESC lines from different parental origins provided a unique opportunity to evaluate the relation between varying levels of imprinted gene expression and DMR methylation status in a cell-line-specific manner. Generally, elevated MEG expression correlated with high methylation levels at M-DMRs and low methylation levels at P-DMRs; vice versa, higher PEG expression correlated with high methylation levels at P-DMRs and low methylation levels at M-DMRs (Figure S2C). Importantly, these patterns were also observed at individual loci for which a regulatory relationship between imprinted genes and DMRs is known (Figures 3A, 3B, and S3). 24 of 26 imprinted genes showed significant correlation between expression and DNA methylation levels of their corresponding DMR (Figure 3C). For most genes, upregulation correlated with DMR hypomethylation, but for five genes upregulation correlated with hypermethylation (negative and positive correlation coefficients, respectively). This contrast was most pronounced at the *KvDMR1* and *H19* loci, each containing one MEG and one PEG that show opposing expression patterns despite being regulated by the same DMR (Figures 3C and S3).

Several imprinted loci showed relatively larger variation in gene expression and DNA methylation levels across different samples. For example, the *MKRN3/MIR4508* DMR, which appears hypermethylated in normal bi-parental human pluripotent stem cells (Ma et al., 2014), was more highly methylated in human aESCs compared with other M-DMRs, but nonetheless hypomethylated relative to bi-parental ESCs and pESCs, correlating with upregulation of its associated PEG *MKRN3* (Figures 2C and S3). Importantly, although imprinting status was largely consistent between cell lines of a given parental origin and across passages (Figure S2D), suggesting stability of imprinted loci in uniparental ESCs, some cell-line-specific differences suggest rare cell-line- and locus-specific aberrations, as previously seen in bi-parental ESC lines (Adewumi et al., 2007; Bar et al., 2017; Frost et al., 2011; Johannesson et al., 2014; Kim et al., 2007a; Ma et al., 2014; Rugg-Gunn et al., 2005, 2007). In line with this notion, aES5 cells seemed to had undergone monoallelic loss of imprinting of *H19* and *IGF2* based on their bi-parental-ESC-like expression levels and DNA methylation of the *H19* DMR, whereas pES12 displayed similar loss of imprinting of *PEG10* and *SGCE*, which are both regulated by the *PEG10* DMR (Figures 2A, 2C, and S3).

Identification of Previously Undescribed Imprinted Genes

Human aESCs, pESCs, and bi-parental ESCs represent the occurrence of different parental backgrounds within the same cell type and differentiation state. Therefore, differences between these cells are likely caused by imprinting, and comparing them

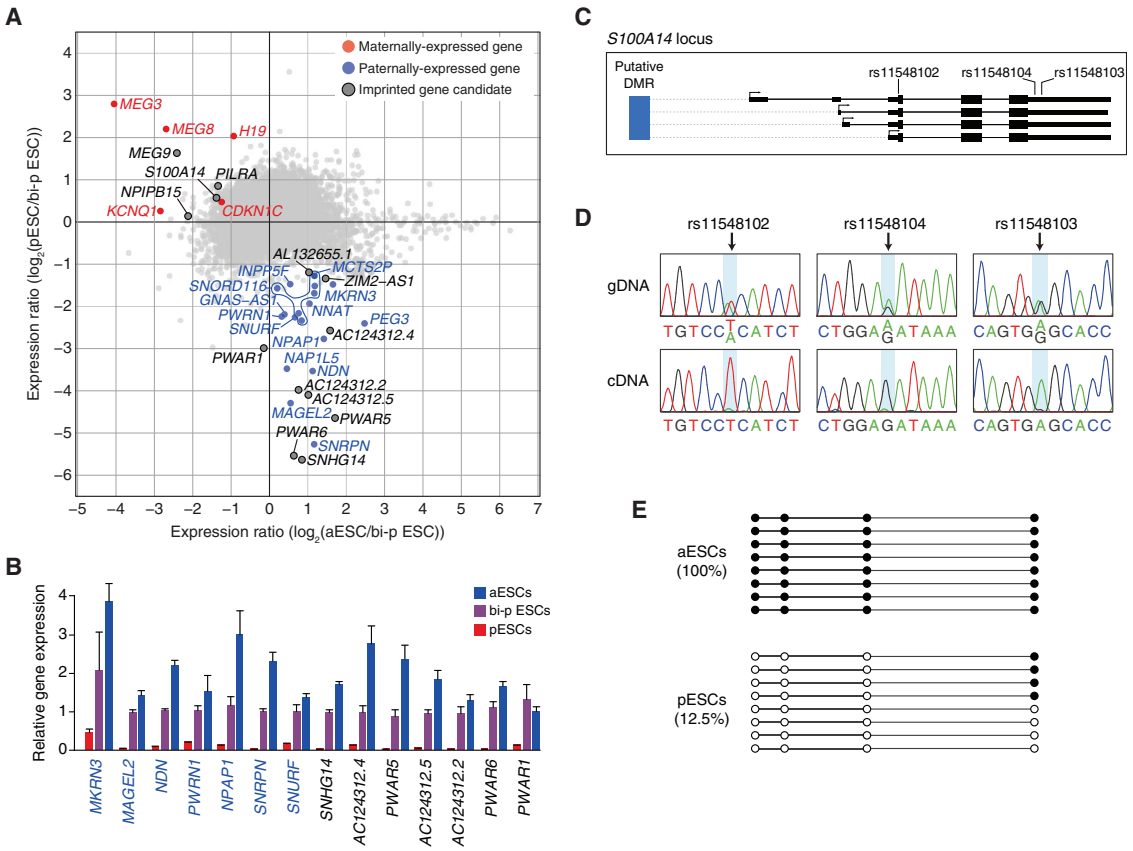

Figure 4. Identification of Imprinted Genes Using Human aESCs, pESCs, and Bi-Parental ESCs

(A) Scatterplot of gene expression ratios between aESCs and bi-parental ESCs (x axis) and pESCs and bi-parental (bi-p) ESCs (y axis; in logarithmic scale, replicates detailed in Table S4). Significantly differentially expressed genes are highlighted. Known MEGs and PEGs appear in red and blue, respectively. Imprinted gene candidates are outlined.

(B) Gene expression levels (mean ± SEM) of known and newly detected imprinted genes (in blue and black annotation, respectively) within the PWS-AS region on chromosome 15 in human aESCs, pESCs, and bi-parental (bi-p) ESCs relative to the median in bi-parental ESCs (replicates detailed in Table S4).

(C) Schematic of the *S100A14* locus, indicating transcriptional variants, SNPs, and upstream putative DMR (see Figure S4C).

(D) Sanger sequencing of heterozygous SNPs within *S100A14* in WA09 cells at the levels of genomic DNA (gDNA) and reverse-transcribed RNA (cDNA).

(E) Bisulfite sequencing analysis of the putative *S100A14* DMR in aESCs (aES3) and pESCs (pES10). Open circles represent unmethylated CpGs and filled circles represent methylated CpGs. Percentage of methylated sites is indicated.

may lead to the identification of previously undescribed imprinted genes and regions in the human genome. In this system, imprinted genes should in principle show unique expression signatures. Relative to bi-parental ESCs, MEGs should appear dramatically downregulated in aESCs and approximately 2-fold upregulated in pESCs, and, likewise, PEGs should be markedly downregulated in pESCs and about 2-fold upregulated in aESCs.

Differential gene expression analysis comparing human aESCs and pESCs with bi-parental ESCs (see STAR Methods) yielded a total of 36 genes with significant parent-of-origin expression signatures (Figure 4A). Of these, 19 were known PEGs and four were known MEGs. The other genes with a paternal expression signature consisted of seven genes localizing within the well-known imprinted region on chromosome 15q11–q13 linked to Prader-Willi syndrome (PWS) and Angelman syndrome (AS), including the recently proposed PEGs *SNHG14*, *PWAR1*, *PWAR5*, and *PWAR6* (Baran et al., 2015) (Figure 4B). Two additional PEG candidates were *ZIM2-AS1*, mapping to the *PEG3–ZIM2* imprinted locus on chromosome 19, and *AL132655.1*, which resides within the *GNAS* imprinted locus on chromosome 20. Genes featuring a maternal expression signature included the recently proposed gene *MEG9* at the *DLK1-DIO3* locus on chromosome 14 (Baran et al., 2015), as well as three additional MEG candidates not associated with known imprinted loci (*S100A14*, *PILRA*, and *NPIPB15*).

In general, genes may exhibit parent-of-origin expression signatures either due to their own imprinting, or as a result of being regulated by imprinted genes in *trans*. For example, a non-imprinted gene would display a MEG-like signature if it were the target of PEG-mediated repression or MEG-mediated induction. However, imprinted genes are distinguished from their targets by virtue of their allele-specific expression. To further characterize the putative MEGs found outside known imprinted regions, we made use of whole-genome sequencing (WGS) data of normal bi-parental ESCs to identify heterozygous single-nucleotide polymorphisms (SNPs) within their transcripts, as well as RNA-seq data to determine whether they are expressed in a monoallelic fashion (see STAR Methods). Informative polymorphisms in

WA09 ESCs (Thomson et al., 1998) were identified within *PILRA* and *S100A14*, but not *NPIPB15*. *PILRA* showed biallelic expression (Figure S4A), suggesting it may be a target gene subject to repression by a PEG or induction by a MEG. However, *S100A14* showed monoallelic expression (Figure S4B), which was also verified by direct cDNA sequencing (Figures 4C and 4D). Notably, upstream of this gene, we identified a putative P-DMR showing intermediate DNA methylation levels across multiple tissues (Figures 4C and S4C) and represented by a CpG site that was hypermethylated in sperm and androgenetic samples, and hypomethylated in parthenogenetic samples (Figure S4D). Direct bisulfite sequencing of this region confirmed its hypermethylation in aESCs and hypomethylation in pESCs (Figure 4E). Moreover, treating aESCs with the demethylating agent 5-aza-2′-deoxycytidine resulted in significant upregulation of *S100A14* to a level comparable with pESCs, consistent with derepression of both alleles (Figure S4E). Together, these data imply that *S100A14*, a putative cancer-related gene encoding a calcium binding protein, is a maternally expressed imprinted gene.

Enhanced Extraembryonic Differentiation of Human aESCs

The reciprocal developmental consequences of androgenesis and parthenogenesis, manifesting almost as mutually exclusive contributions to either extraembryonic or embryonic lineages, are thought to reflect intrinsic differentiation propensities of the paternal and maternal genomes (Barton et al., 1984; Kajii and Ohama, 1977; Kaufman et al., 1977; Linder et al., 1975; McGrath and Solter, 1984; Surani and Barton, 1983; Surani et al., 1984, 1986). To test whether human aESCs show enhanced extraembryonic differentiation, we took advantage of the ability to perform directed differentiation of human ESCs into trophoblast cells and implemented it on human aESCs, pESCs, and bi-parental ESCs. Notably, although this differentiation resulted in upregulation of placental-enriched genes in all three cell types compared with their undifferentiated counterparts, expression levels of these genes following differentiation were lower in pESCs relative to bi-parental ESCs and significantly elevated in aESCs (Figures 5A and 5B). Upregulated genes showing this pattern included hallmarks of trophoblast differentiation, such as those encoding chorionic gonadotrophins (*CGA* and *CGB8*) and fusogenic endogenous retroviral envelope proteins (*ERVFRD-1* and *ERVW-1*). These results indicate that the paternal-genome bias toward extraembryonic differentiation is recapitulated by trophoblast differentiation *in vitro*. Importantly, the imprinted PEG *IGF2*, which plays an important role in placental development (Constância et al., 2002), was absent in differentiated pESCs but markedly upregulated in differentiated aESCs (Figure 5A). This differential expression of *IGF2*, as well as that of its regulators *IGFBP3* and *PAPPA2*, may at least partially explain this phenotype.

A Paternal-Genome Bias toward Liver Differentiation

To identify additional developmental biases driven by parent-of-origin effects, we utilized the pluripotency of our three different types of human ESC lines to generate teratomas *in vivo* and compare their differentiation propensities. To this end, we assessed the expression levels of the most enriched genes across 22 human tissues that represented a variety of endodermal, ectodermal, and mesodermal lineages (Figures 5C and S5A; Tables S4 and S6; see STAR Methods). Considering the heterogeneity and variability associated with teratoma differentiation, we analyzed a total of nine independent teratomas derived from three aESC lines, two pESC lines and two bi-parental ESC lines (see Table S4).

Teratomas differentiated from human aESCs and pESCs showed significant differences in tissue-enriched gene expression. The most pronounced and consistent difference was observed with liver-enriched genes, which were upregulated in aESC-derived teratomas and downregulated in pESC-derived teratomas (Figures 5C and 5D). Furthermore, genes with significantly elevated expression in aESC-derived teratomas compared with those from both bi-parental ESCs and pESCs (false discovery rate [FDR] <0.05 and fold change >2 by both comparisons) were highly overrepresented by liver genes such as *ALB*, *HP*, *ITIH1*, and *ADH1A* (12 genes of 20, corrected $p = 3.90 \times 10^{-6}$). Other endodermal lineages showed a similar trend, with significant increase in the expression of pancreas and gallbladder genes in androgenetic teratomas (Figure 5C).

An opposite bias was detected in the expression levels of cerebral-cortex enriched genes, which were significantly increased in teratomas of pESC origin and reduced in those of aESC origin, suggesting that lacking a maternal-genome impedes efficient differentiation toward neuronal lineages (Figure 5C). Aside from a small increase in the expression of testis-enriched genes in teratomas from pESCs relative to those from aESCs, parent-specific differentiation biases were not observed for other mesodermal tissues. Notably, both aESC- and pESC-derived teratomas showed marked downregulation of skeletal-muscle enriched genes relative to those from bi-parental ESCs. In addition, genes with significantly increased expression in bi-parental ESC-derived teratomas (FDR <0.05 and fold change >2 by both comparisons) were highly enriched for skeletal muscle genes (9 genes of 13, corrected $p = 4.10 \times 10^{-9}$). In the mouse, deficiency in skeletal muscle development was specifically observed in parthenogenetic cells (Barton et al., 1991; Fundele et al., 1989, 1990; Nagy et al., 1989). Our results suggest that in humans, the paternal and maternal genomes in bi-parental cells are not merely additive in their effect but have complementary contributions to muscle differentiation.

The strong paternal-genome bias toward liver development that clearly emerged from our analysis of spontaneous multi-lineage differentiation *in vivo*, prompted us to test it further by performing directed hepatic differentiation of additional human aESCs, bi-parental ESCs and pESCs *in vitro*. RNA-seq-based PCA demonstrated that while hepatic differentiation induced an exit from the pluripotent state in all ESC types (negative PC1 values), it had a differential effect on aESCs and pESCs causing their separation across PC2, with differentiated cells from bi-parental ESCs found mostly in between (Figure 6A). Furthermore, differentiated aESCs showed a typical hepatocyte-like morphology and were stained for the liver markers AFP and albumin, whereas differentiated pESCs had a variable and undefined morphology and showed no detectable expression of these markers (Figure 6B). Single-cell quantification indicated that the majority of aESCs, but none of the pESCs had differentiated into hepatic cells expressing high levels of albumin (Figure S5B).

Consistent with these observations, liver-enriched genes upregulated in hepatic differentiation of normal bi-parental ESCs

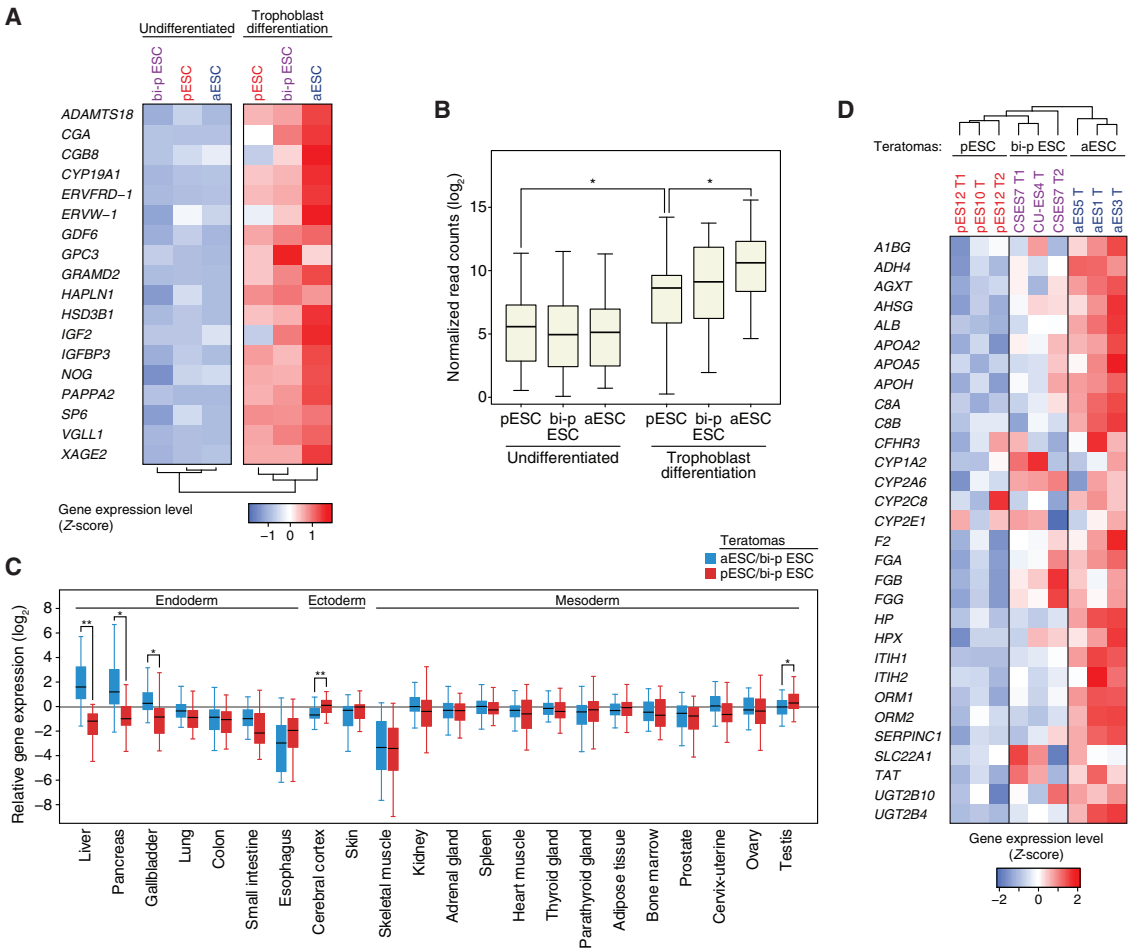

Figure 5. Lineage Biases of Human aESCs and pESCs in Directed Trophoblast Differentiation and Teratoma Formation

(A) Mean expression of placenta-enriched genes upregulated during trophoblast differentiation of human aESCs, pESCs, and bi-parental (bi-p) ESCs (replicates detailed in Table S4).

(B) Expression levels of the genes shown in 5B (logarithmic scale). *p < 0.05 (two-tailed unpaired Student's t test).

(C) Expression levels of the top 30 tissue-enriched genes for 22 human tissues, in teratomas from human aESCs (blue) and pESCs (red) relative to those from bi-parental (bi-p) ESCs (in logarithmic scale, n = 3 in each group; see Tables S4 and S6 and STAR Methods for sample identities, gene lists, and analysis details). *p < 0.05, **p < 0.01, ***p < 0.001 (two-tailed unpaired Student's t test).

(D) Expression levels of the top 30 liver-enriched genes in different teratomas from human aESCs, pESCs, and bi-parental (bi-p) ESCs.

(encoding multiple carrier proteins, other plasma secreted proteins, coagulation regulators, and liver enzymes) were highly upregulated in differentiated aESCs, but to a much lesser extent in differentiated pESCs, which reached expression levels that were more reminiscent of those in undifferentiated cells (Figures 6C and 6D). During development, many liver genes are also expressed in the extraembryonic yolk sac. However, of the 41 hepatic differentiation genes analyzed, only 14 (34%) were previously shown to be expressed in both tissues (Cindrova-Davies et al., 2017). Moreover, whereas liver-unique genes and genes shared between the liver and yolk sac were overall markedly upregulated in differentiated aESCs, yolk-sac unique genes were similarly expressed in differentiated aESCs and pESCs (Figure S5C), illustrating that the paternal-genome bias observed is specific to hepatic differentiation. Genes encoding hepatic transcription factors (Sheaffer and Kaestner, 2012) were downregulated in differentiated pESCs and in most cases upregulated in differentiated aESCs relative to differentiated bi-parental ESCs (Figure 6E), indicating robust rewiring of the transcriptional network to conform with hepatic cell identity. Taken together, these results emphasize a strong proficiency of androgenetic cells for hepatic differentiation *in vivo* and *in vitro*, suggesting that the paternal genome promotes liver development.

The Paternally Expressed Gene *IGF2* Plays a Prominent Role in Liver Differentiation

The contrast between the marked proficiency of aESCs and considerable deficiency of pESCs in differentiation into hepatic cells points to a mechanistic role for imprinted genes in driving this parent-specific bias. In particular, we predicted that PEGs, with elevated expression in aESCs and no expression in pESCs, likely account for this phenotype. To explore the involvement of specific PEGs, we analyzed changes in the expression levels of all known PEGs following hepatic differentiation of normal

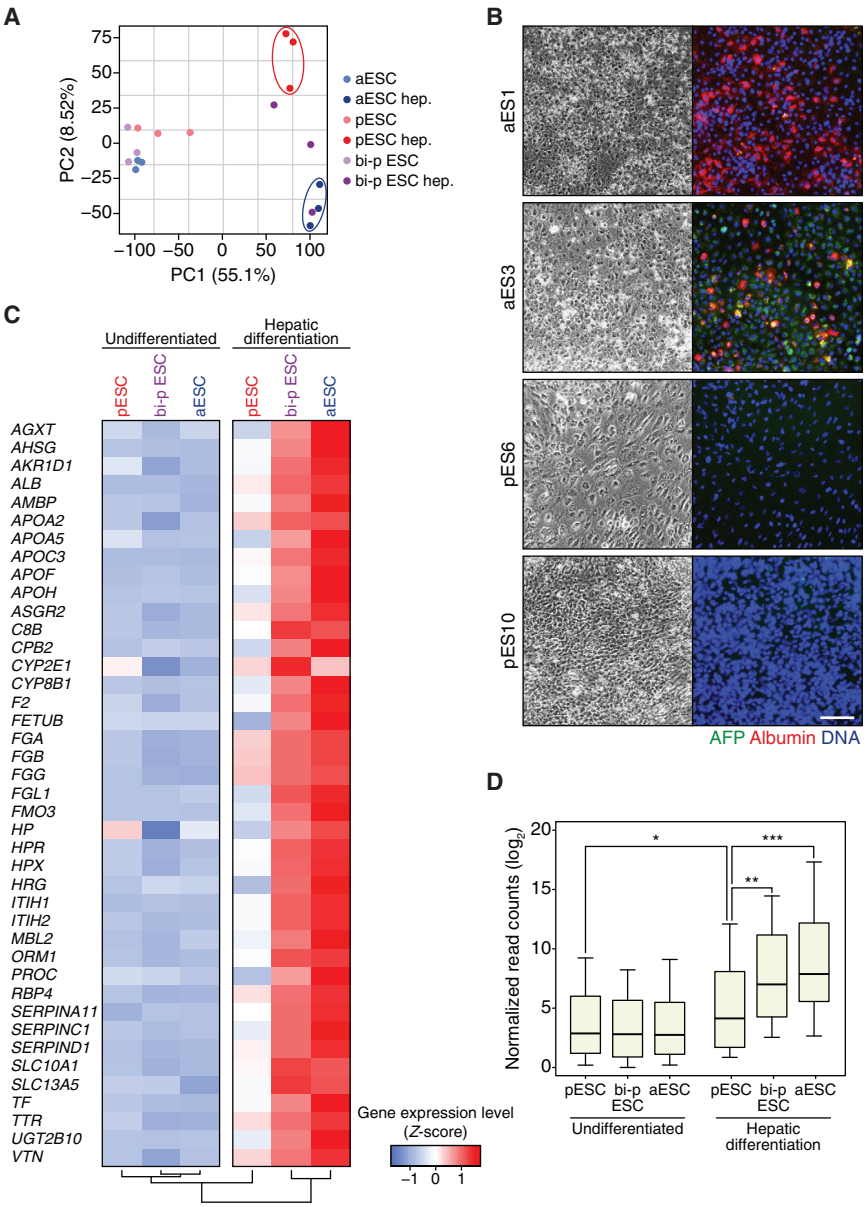

Figure 6. Directed Hepatic Differentiation Demonstrates the Liver-Contribution Proficiency of aESCs

(A) PCA of global gene expression in undifferentiated and hepatic-differentiated (hep.) human aESCs, pESCs, and bi-parental ESCs (replicates detailed in Table S4). Percentages of explained variation are indicated in parentheses.

(B) Morphology and immunofluorescence staining of AFP (green), albumin (red), and DNA (blue) in human aESCs and pESCs following hepatic differentiation. Scale bar, 100 μm (see Figure S5B).

(C) Mean expression of liver-enriched genes upregulated in hepatic differentiation of human aESCs, pESCs, and bi-parental ESCs (replicates detailed in Table S4).

(D) Expression levels of the genes shown in 6C (logarithmic scale). *$p < 0.05$, **$p < 0.01$, ***$p < 0.001$ (two-tailed unpaired Student's t test).

(E) Relative expression (mean ± SEM) of hepatic transcription factor genes in hepatic-differentiated (hep.) human aESCs, pESCs, and bi-parental ESCs (n = 3 for each group, replicates detailed in Table S4). *$p < 0.05$, **$p < 0.01$, ***$p < 0.001$ (two-tailed unpaired Student's t test).

Bi-p, bi-parental.

bi-parental ESCs (Figure 7A). Whereas the vast majority of PEGs showed little or no change in expression upon differentiation, *IGF2* stood out as the most upregulated gene (mean fold change of nearly 250), hinting to its importance in this process. As expected, *IGF2* was exceedingly upregulated upon differentiation of human aESCs but was only negligibly expressed in pESCs both prior to and following differentiation (Figure 7B). Interestingly, Beckwith-Wiedemann syndrome patients, which similar to aESCs sometimes show biallelic expression of *IGF2* and silencing of *H19*, display abnormal enlargement of the liver and increased rate of hepatoblastoma (Weksberg et al., 2010), suggesting the involvement of paternal imprinting at this locus in liver development.

To interrogate the functional role of *IGF2* in liver differentiation, we generated two individual *IGF2*-knockout (KO) aESC lines in both aES1 and aES3 cell lines by CRISPR-Cas9 with a single-guide RNA (sgRNA) targeting a constitutively expressed exon (Figures 7C and S6). Both KO cell lines harbored disruptive *IGF2* mutations due to frameshift deletions. Subsequently, we subjected control wild-type (WT) and *IGF2*-KO aESCs to directed hepatic differentiation followed by RNA-seq analysis. Genes significantly downregulated in *IGF2*-KO aESCs compared with WT aESCs (FDR <0.05 and fold change >2) were highly enriched for liver- (79 genes of 398, corrected $p = 1.4 \times 10^{-9}$) and plasma-related genes (31 genes of 398, corrected $p = 1.8 \times 10^{-13}$) (Figure 7D). Importantly, all 41 genes initially defined as liver-enriched and normally upregulated in hepatic differentiation of bi-parental ESCs (Figure 6C) were downregulated in differentiated *IGF2*-KO aESCs, of which 17 were significantly downregulated (Figures 7E and 7F). These findings

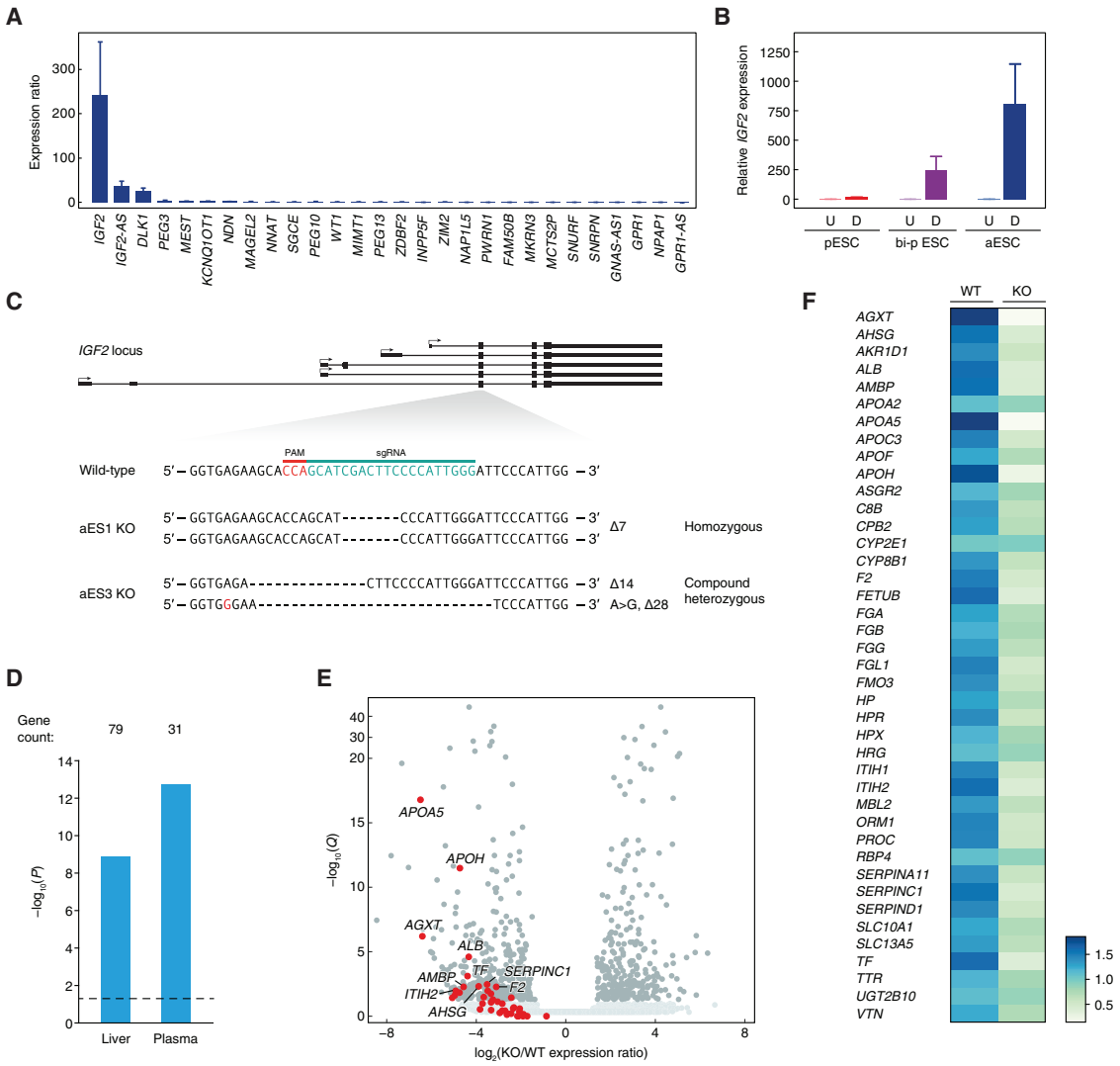

Figure 7. Involvement of the Imprinted Gene *IGF2* in Hepatic Differentiation of Human aESCs

(A) Change in expression levels of known PEGs following hepatic differentiation of human bi-parental ESCs (mean ± SEM relative to the mean level in undifferentiated cells, n = 3, replicates detailed in Table S4).

(B) *IGF2* expression (mean ± SEM) in undifferentiated (U) and differentiated (D) human pESCs, bi-parental (bi-p) ESCs, and aESCs following hepatic differentiation (n = 3 for each group, replicates detailed in Table S4).

(C) Schematic of the *IGF2* locus, sgRNA targeting site, and sequences of *IGF2*-KO human aESC lines (also see Figure S6). PAM, protospacer adjacent motif; Δ, deletion.

(D) Functional annotation enrichment analysis of downregulated genes in *IGF2*-KO aESCs compared with WT aESCs. Dashed line indicates corrected p value of 0.05.

(E) Log-scaled volcano plot of differential gene expression between *IGF2*-KO and WT human aESCs. Significantly downregulated and upregulated genes (greater than 2-fold change, *Q* (FDR) < 0.05) are marked in dark gray. Liver-enriched genes upregulated during hepatic differentiation of normal bi-parental ESCs (from Figure 6C) are marked in red. (replicates detailed in Table S4).

(F) Mean expression of liver-enriched genes upregulated in hepatic differentiation, in *IGF2*-KO and WT human aESCs (replicates detailed in Table S4).

demonstrate the importance of the imprinted gene *IGF2* in liver differentiation, implicating its proper expression as part of the molecular mechanism underlying the paternal-genome bias toward this lineage.

DISCUSSION

Understanding the functional impact that imprinting bears on human development and disease is of major interest. In this study, we established a collection of human ESCs representing all instances of parental origin, consisting of newly derived aESCs, pESCs, and bi-parental ESCs. Although we and others have previously derived human parthenogenetic pluripotent stem cells (Brevini et al., 2009; Kim et al., 2007b; Revazova et al., 2007; Sagi et al., 2016a; Stelzer et al., 2011), the ability to generate human aESCs has been demonstrated in only one study reporting a single cell line (Ding et al., 2015). Here, we derived six individual human aESC lines from three independent donors and

characterized their molecular and cellular properties. Human aESCs, pESCs, and bi-parental ESCs are all pluripotent and correspond to the same cell type and global regulatory landscape. Yet, they are readily discerned by unique imprinting signatures, indicating that manipulations and culturing did not have a substantial impact on their overall imprinting status. We therefore utilized these cells as a unique experimental system for systematic dissection of different aspects of imprinting in isolated parental backgrounds, including the identification of previously undescribed imprinted genes and analysis of parent-specific developmental implications.

Comparing uniparental and bi-parental cells by genome-wide methodologies is useful for identifying imprinted genes. In the mouse, subtraction-hybridization between cDNAs from normal and either parthenogenetic or androgenetic embryos led to the initial identification of several imprinted genes (Ishino et al., 2001; Kaneko-Ishino et al., 1995; Miyoshi et al., 1998). We previously compared human all-maternal parthenogenetic and bi-parental pluripotent stem cells and identified both known and previously unknown PEGs due to their marked downregulation in parthenogenetic cells (Stelzer et al., 2011, 2013, 2015). Here, the addition of all-paternal human aESCs representing the opposite extreme provided us with enhanced resolution for detecting imprinted genes. Although our results suggest that the majority of imprinted genes expressed in human ESCs have been described before, they also pointed to the existence of undescribed imprinted genes, mainly within (e.g., *ZIM2-AS1*) but also outside known imprinted regions (*S100A14*). It is possible that additional imprinted genes, especially ones with more complex tissue- or isoform-specific regulation (Stelzer et al., 2015), remain to be discovered.

Although it is well established that imprinting exerts a crucial influence on mammalian development, the functional roles of each parental genome in humans are not known. Consistent with the notion that the paternal and maternal genomes are reciprocally biased toward extraembryonic and embryonic lineages, we found that trophoblast differentiation of human aESCs shows an intrinsic bias toward placental development. In future studies, this system may facilitate the modeling of androgenetic hydatidiform mole formation.

The effects of uniparental development in the mouse can only be analyzed until mid-gestation as early placental and embryonic defects impede further embryogenesis (McGrath and Solter, 1984; Surani and Barton, 1983; Surani et al., 1984). Chimerism assays combining normal and uniparental cells partially overcome this limitation, allowing the detection of parent-of-origin-driven biases in contribution to various tissues (Barton et al., 1991; Fundele et al., 1989, 1990; Mann et al., 1990; Nagy et al., 1989). Nonetheless, incorporation of uniparental cells in chimeras result in severe abnormalities and lethality (Barton et al., 1991; Mann et al., 1990), and the extent of uniparental-cell contribution may be influenced by differences in proliferation rates or survival of these cells rather than indicating inherent differentiation capacity (Fundele et al., 1990).

Here, we utilized teratoma formation, which entails heterogenous *in vivo* differentiation into numerous tissues independent of coordinated development, to analyze cell-autonomous differentiation propensities of uniparental ESCs. Remarkably, this approach alluded to parent-specific biases in several tissues. The most prominent bias was reflected by the marked proficiency of the paternal genome and deficiency of the maternal genome toward liver differentiation, as also confirmed by directed hepatic differentiation. These findings emphasize an intrinsic competence of the paternal genome to contribute to both extraembryonic and certain embryonic lineages. Our data may support the parental conflict theory of imprinting (Moore and Haig, 1991), by which paternal genes increase fetal fitness by maximizing consumption of maternal resources, as androgenetic cells show robust differentiation into the liver, which is the largest internal organ and a central site of metabolism.

In contrast, neuronal differentiation was less promptly detectable in teratomas from aESCs compared with those from pESCs. Notably, both biases are consistent with reports on impaired liver differentiation and enhanced brain differentiation of mouse and human parthenogenetic cells (Barton et al., 1991; Fundele et al., 1989, 1990; Nagy et al., 1989; Stelzer et al., 2011). Thus, in certain tissues such as the liver and brain, the paternal and maternal genomes can show an opposite phenotype, implying the involvement of imprinted genes that are absent from one genome and overexpressed from the other. Furthermore, although skeletal muscle differentiation is considered specifically compromised in parthenogenetic mouse cells (Barton et al., 1991; Fundele et al., 1989, 1990; Nagy et al., 1989), our data suggest that both parental genomes are required for proper differentiation of this tissue, implying that imprinted genes involved in differentiation of some tissues may be uniquely expressed from each of the parental genomes. In future studies, directed muscle differentiation of mouse and human uniparental cells will help resolve whether this observation arises from interspecies differences.

How imprinting is mechanistically involved in the regulation of parent-specific differentiation biases is highly intriguing. We demonstrated that *IGF2*, the most upregulated PEG in normal hepatic differentiation, plays a key role in this process, as *IGF2*-KO aESCs displayed distinct molecular signatures consistent with impaired liver specification upon differentiation. It is therefore likely that differential regulation of *IGF2* in androgenetic and parthenogenetic cells at least partially underlies the paternal-genome bias toward this lineage. Furthermore, this finding may be of clinical significance, as biallelic expression of *IGF2*, which is associated with certain cases of Beckwith-Wiedemann syndrome, might account for the liver enlargement and increased rate of hepatoblastoma observed in these patients (Weksberg et al., 2010).

Analyzing the differentiation potential of uniparental ESCs may have additional clinical implications. As parthenogenetic and androgenetic gestations occur spontaneously in women and develop into ovarian teratomas and hydatidiform moles (Kajii and Ohama, 1977; Linder et al., 1975), our resource may enable more faithful modeling of these tumors using human cells. Furthermore, although fully uniparental embryos are non-viable, in rare cases, uniparental cells may exist in newborns as mosaics of normal and either parthenogenetic or androgenetic cells (Kotzot, 2008; Lapunzina and Monk, 2011). These children show severe developmental abnormalities, and affected tissues can now

be studied based on our differentiation assay of uniparental ESCs.

The uniparental origin and pluripotency of human aESCs and pESCs make them a valuable resource for future studies on imprinting. They can be utilized for studying regulatory mechanisms at known imprinted loci, as both their alleles feature the same parent-specific epigenetic and transcriptional status. Gaining further insight into imprinting regulation may also be useful for generating blastocyst-like naive human pluripotent stem cells, which under current culture conditions undergo global and irreversible imprinting erasure (Pastor et al., 2016; Theunissen et al., 2016). Furthermore, human aESCs and pESCs can also be employed for modeling developmental disorders and cancers associated with aberrant imprinting at either specific loci or globally as in ovarian teratomas and hydatidiform moles.

We anticipate that human ESCs from distinct parental backgrounds will shed light on the functional non-equivalence of parental genomes and provide new insights into the significance of imprinting in human development and disease.

STAR★METHODS

Detailed methods are provided in the online version of this paper and include the following:

- KEY RESOURCES TABLE
- LEAD CONTACT AND MATERIALS AVAILABILITY
- EXPERIMENTAL MODEL AND SUBJECT DETAILS
  - Human subjects
  - Animals
  - Cell lines
- METHOD DETAILS
  - Oocyte donation
  - Sperm donation and processing
  - *In vitro* androgenesis
  - Derivation of human ESC lines
  - Short tandem repeat analysis
  - Karyotype analysis
  - Immunofluorescence and alkaline phosphatase staining
  - Teratoma formation assay
  - RNA sequencing
  - Expression analysis of known imprinted genes
  - Expression analysis of previously undescribed imprinted genes
  - Global DNA methylation analysis
  - Bisulfite sequencing analysis
  - DNA demethylation analysis
  - Trophoblast differentiation
  - Hepatic differentiation
  - Analyses of tissue-enriched gene expression
  - Generation and analysis of *IGF2*-knockout aESC lines
- QUANTIFICATION AND STATISTICAL ANALYSIS
- DATA AND CODE AVAILABILITY

SUPPLEMENTAL INFORMATION

Supplemental Information can be found online at https://doi.org/10.1016/j.stem.2019.06.013.

ACKNOWLEDGMENTS

We thank all members of the Egli and Benvenisty laboratories for valuable input. We thank D. Vershkov for advice in histological analysis, and U. Weissbein, Y. Avior, and S. Bar for help in allele-specific analysis using WGS and RNA-seq data. I.S. is supported by the Adams Fellowships Program for Doctoral Students; N.B. is the Herbert Cohn Chair in Cancer Research. This work was partially supported by the US-Israel Binational Science Foundation (grant no. 2015089), by the Israel Science Foundation (grant no. 494/17), by the Azrieli Foundation (to N.B.); by the NYSCF-Robertson Stem Cell Investigator award; and by the NYSTEM award #C32564GG (to D.E.).

AUTHOR CONTRIBUTIONS

I.S., J.C.D.P., N.B., and D.E. conceived the study and wrote the manuscript with input from all authors. I.S. characterized human aESC lines, generated *IGF2*-knockout cells, performed differentiation experiments, and analyzed the data. J.C.D.P. recruited gamete donors and performed sperm preparation. M.V.Z. assisted with the derivation of human aESC lines and generation of STR profiles. C.A. assisted with histological analysis. T.G.-L. performed karyotype analysis. O.Y. assisted with cell culture. R.P., A.S., and D.E. performed ICSI and oocyte enucleation. G.P. prepared samples for DNA methylation analysis. T.C., B.G., S.H.T., and R.G. recruited gamete donors. M.V.S. and R.L. performed oocyte donor recruitment and oocyte aspirations. D.E. derived human ESC lines. N.B. and D.E. supervised the study.

DECLARATION OF INTERESTS

N.B. is CSO of NewStem Ltd.

Received: June 14, 2018
Revised: March 17, 2019
Accepted: June 18, 2019
Published: September 5, 2019

SUPPORTING CITATIONS

The following references appear in the Supplemental Information: Duffié et al. (2014); Madan and Bobrow (1974).

REFERENCES

Adewumi, O., Aflatoonian, B., Ahrlund-Richter, L., Amit, M., Andrews, P.W., Beighton, G., Bello, P.A., Benvenisty, N., Berry, L.S., Bevan, S., et al.; International Stem Cell Initiative (2007). Characterization of human embryonic stem cell lines by the International Stem Cell Initiative. Nat. Biotechnol. *25*, 803–816.

Amita, M., Adachi, K., Alexenko, A.P., Sinha, S., Schust, D.J., Schulz, L.C., Roberts, R.M., and Ezashi, T. (2013). Complete and unidirectional conversion of human embryonic stem cells to trophoblast by BMP4. Proc. Natl. Acad. Sci. USA *110*, E1212–E1221.

Anders, S., Pyl, P.T., and Huber, W. (2015). HTSeq–a Python framework to work with high-throughput sequencing data. Bioinformatics *31*, 166–169.

Avior, Y., Levy, G., Zimerman, M., Kitsberg, D., Schwartz, R., Sadeh, R., Moussaieff, A., Cohen, M., Itskovitz-Eldor, J., and Nahmias, Y. (2015). Microbial-derived lithocholic acid and vitamin K2 drive the metabolic maturation of pluripotent stem cells-derived and fetal hepatocytes. Hepatology *62*, 265–278.

Bar, S., Schachter, M., Eldar-Geva, T., and Benvenisty, N. (2017). Large-scale analysis of loss of imprinting in human pluripotent stem cells. Cell Rep. *19*, 957–968.

Baran, Y., Subramaniam, M., Biton, A., Tukiainen, T., Tsang, E.K., Rivas, M.A., Pirinen, M., Gutierrez-Arcelus, M., Smith, K.S., Kukurba, K.R., et al.; GTEx Consortium (2015). The landscape of genomic imprinting across diverse adult human tissues. Genome Res. *25*, 927–936.

Barlow, D.P., and Bartolomei, M.S. (2014). Genomic imprinting in mammals. Cold Spring Harb. Perspect. Biol. *6*, a018382.

Barton, S.C., Surani, M.A., and Norris, M.L. (1984). Role of paternal and maternal genomes in mouse development. Nature *311*, 374–376.

Barton, S.C., Ferguson-Smith, A.C., Fundele, R., and Surani, M.A. (1991). Influence of paternally imprinted genes on development. Development *113*, 679–687.

Brevini, T.A.L., Pennarossa, G., Antonini, S., Paffoni, A., Tettamanti, G., Montemurro, T., Radaelli, E., Lazzari, L., Rebulla, P., Scanziani, E., et al. (2009). Cell lines derived from human parthenogenetic embryos can display aberrant centriole distribution and altered expression levels of mitotic spindle check-point transcripts. Stem Cell Rev. *5*, 340–352.

Carpenter, A.E., Jones, T.R., Lamprecht, M.R., Clarke, C., Kang, I.H., Friman, O., Guertin, D.A., Chang, J.H., Lindquist, R.A., Moffat, J., et al. (2006). CellProfiler: image analysis software for identifying and quantifying cell phenotypes. Genome Biol. *7*, R100.

Chen, A.E., Egli, D., Niakan, K., Deng, J., Akutsu, H., Yamaki, M., Cowan, C., Fitz-Gerald, C., Zhang, K., Melton, D.A., and Eggan, K. (2009). Optimal timing of inner cell mass isolation increases the efficiency of human embryonic stem cell derivation and allows generation of sibling cell lines. Cell Stem Cell *4*, 103–106.

Cindrova-Davies, T., Jauniaux, E., Elliot, M.G., Gong, S., Burton, G.J., and Charnock-Jones, D.S. (2017). RNA-seq reveals conservation of function among the yolk sacs of human, mouse, and chicken. Proc. Natl. Acad. Sci. *114*, E4753 LP-E4761.

Constância, M., Hemberger, M., Hughes, J., Dean, W., Ferguson-Smith, A., Fundele, R., Stewart, F., Kelsey, G., Fowden, A., Sibley, C., and Reik, W. (2002). Placental-specific IGF-II is a major modulator of placental and fetal growth. Nature *417*, 945–948.

Cooper, T.G., Noonan, E., von Eckardstein, S., Auger, J., Baker, H.W.G., Behre, H.M., Haugen, T.B., Kruger, T., Wang, C., Mbizvo, M.T., and Vogelsong, K.M. (2010). World Health Organization reference values for human semen characteristics. Hum. Reprod. Update *16*, 231–245.

Court, F., Tayama, C., Romanelli, V., Martin-Trujillo, A., Iglesias-Platas, I., Okamura, K., Sugahara, N., Simón, C., Moore, H., Harness, J.V., et al. (2014). Genome-wide parent-of-origin DNA methylation analysis reveals the intricacies of human imprinting and suggests a germline methylation-independent mechanism of establishment. Genome Res. *24*, 554–569.

Ding, C., Huang, S., Qi, Q., Fu, R., Zhu, W., Cai, B., Hong, P., Liu, Z., Gu, T., Zeng, Y., et al. (2015). Derivation of a homozygous human androgenetic embryonic stem cell line. Stem Cells Dev. *24*, 2307–2316.

Dobin, A., Davis, C.A., Schlesinger, F., Drenkow, J., Zaleski, C., Jha, S., Batut, P., Chaisson, M., and Gingeras, T.R. (2013). STAR: ultrafast universal RNA-seq aligner. Bioinformatics *29*, 15–21.

Duffié, R., Ajjan, S., Greenberg, M.V., Zamudio, N., Escamilla del Arenal, M., Iranzo, J., Okamoto, I., Barbaux, S., Fauque, P., and Bourc'his, D. (2014). The Gpr1/Zdbf2 locus provides new paradigms for transient and dynamic genomic imprinting in mammals. Genes Dev. *28*, 463–478.

Frost, J., Monk, D., Moschidou, D., Guillot, P.V., Stanier, P., Minger, S.L., Fisk, N.M., Moore, H.D., and Moore, G.E. (2011). The effects of culture on genomic imprinting profiles in human embryonic and fetal mesenchymal stem cells. Epigenetics *6*, 52–62.

Fundele, R., Norris, M.L., Barton, S.C., Reik, W., and Surani, M.A. (1989). Systematic elimination of parthenogenetic cells in mouse chimeras. Development *106*, 29–35.

Fundele, R.H., Norris, M.L., Barton, S.C., Fehlau, M., Howlett, S.K., Mills, W.E., and Surani, M.A. (1990). Temporal and spatial selection against parthenogenetic cells during development of fetal chimeras. Development *108*, 203–211.

Goto, H., Yasui, Y., Nigg, E.A., and Inagaki, M. (2002). Aurora-B phosphorylates Histone H3 at serine28 with regard to the mitotic chromosome condensation. Genes Cells *7*, 11–17.

Huang, W., Sherman, B.T., and Lempicki, R.A. (2009). Systematic and integrative analysis of large gene lists using DAVID bioinformatics resources. Nat. Protoc. *4*, 44–57.

Ishino, F., Kuroiwa, Y., Miyoshi, N., Kobayashi, S., Kohda, T., and Kaneko-Ishino, T. (2001). Subtraction-hybridization method for the identification of imprinted genes. Methods Mol. Biol. *181*, 101–112.

Johannesson, B., Sagi, I., Gore, A., Paull, D., Yamada, M., Golan-Lev, T., Li, Z., LeDuc, C., Shen, Y., Stern, S., et al. (2014). Comparable frequencies of coding mutations and loss of imprinting in human pluripotent cells derived by nuclear transfer and defined factors. Cell Stem Cell *15*, 634–642.

Kajii, T., and Ohama, K. (1977). Androgenetic origin of hydatidiform mole. Nature *268*, 633–634.

Kaneko-Ishino, T., Kuroiwa, Y., Miyoshi, N., Kohda, T., Suzuki, R., Yokoyama, M., Viville, S., Barton, S.C., Ishino, F., and Surani, M.A. (1995). *Peg1/Mest* imprinted gene on chromosome 6 identified by cDNA subtraction hybridization. Nat. Genet. *11*, 52–59.

Kaufman, M.H., Barton, S.C., and Surani, M.A. (1977). Normal postimplantation development of mouse parthenogenetic embryos to the forelimb bud stage. Nature *265*, 53–55.

Kaufman, M.H., Robertson, E.J., Handyside, A.H., and Evans, M.J. (1983). Establishment of pluripotential cell lines from haploid mouse embryos. J. Embryol. Exp. Morphol. *73*, 249–261.

Kim, K.-P., Thurston, A., Mummery, C., Ward-van Oostwaard, D., Priddle, H., Allegrucci, C., Denning, C., and Young, L. (2007a). Gene-specific vulnerability to imprinting variability in human embryonic stem cell lines. Genome Res. *17*, 1731–1742.

Kim, K., Lerou, P., Yabuuchi, A., Lengerke, C., Ng, K., West, J., Kirby, A., Daly, M.J., and Daley, G.Q. (2007b). Histocompatible embryonic stem cells by parthenogenesis. Science *315*, 482–486.

Kim, D., Pertea, G., Trapnell, C., Pimentel, H., Kelley, R., and Salzberg, S.L. (2013). TopHat2: accurate alignment of transcriptomes in the presence of insertions, deletions and gene fusions. Genome Biol. *14*, R36.

Kotzot, D. (2008). Complex and segmental uniparental disomy updated. J. Med. Genet. *45*, 545–556.

Lapunzina, P., and Monk, D. (2011). The consequences of uniparental disomy and copy number neutral loss-of-heterozygosity during human development and cancer. Biol. Cell *103*, 303–317.

Lee, J.T., and Bartolomei, M.S. (2013). X-inactivation, imprinting, and long noncoding RNAs in health and disease. Cell *152*, 1308–1323.

Li, H., and Durbin, R. (2009). Fast and accurate short read alignment with Burrows-Wheeler transform. Bioinformatics *25*, 1754–1760.

Linder, D., McCaw, B.K., and Hecht, F. (1975). Parthenogenic origin of benign ovarian teratomas. N. Engl. J. Med. *292*, 63–66.

Love, M.I., Huber, W., and Anders, S. (2014). Moderated estimation of fold change and dispersion for RNA-seq data with DESeq2. Genome Biol. *15*, 550.

Ma, H., Morey, R., O'Neil, R.C., He, Y., Daughtry, B., Schultz, M.D., Hariharan, M., Nery, J.R., Castanon, R., Sabatini, K., et al. (2014). Abnormalities in human pluripotent cells due to reprogramming mechanisms. Nature *511*, 177–183.

Madan, K., and Bobrow, M. (1974). Structural variation in chromosome No 9. Ann. Genet. *17*, 81–86.

Mann, J.R., Gadi, I., Harbison, M.L., Abbondanzo, S.J., and Stewart, C.L. (1990). Androgenetic mouse embryonic stem cells are pluripotent and cause skeletal defects in chimeras: implications for genetic imprinting. Cell *62*, 251–260.

Marchand, M., Horcajadas, J.A., Esteban, F.J., McElroy, S.L., Fisher, S.J., and Giudice, L.C. (2011). Transcriptomic signature of trophoblast differentiation in a human embryonic stem cell model. Biol. Reprod. *84*, 1258–1271.

McGrath, J., and Solter, D. (1984). Completion of mouse embryogenesis requires both the maternal and paternal genomes. Cell *37*, 179–183.

McKenna, A., Hanna, M., Banks, E., Sivachenko, A., Cibulskis, K., Kernytsky, A., Garimella, K., Altshuler, D., Gabriel, S., Daly, M., and DePristo, M.A. (2010). The Genome Analysis Toolkit: a MapReduce framework for analyzing next-generation DNA sequencing data. Genome Res. *20*, 1297–1303.

Miyoshi, N., Kuroiwa, Y., Kohda, T., Shitara, H., Yonekawa, H., Kawabe, T., Hasegawa, H., Barton, S.C., Surani, M.A., Kaneko-Ishino, T., and Ishino, F. (1998). Identification of the *Meg1/Grb10* imprinted gene on mouse proximal

chromosome 11, a candidate for the Silver-Russell syndrome gene. Proc. Natl. Acad. Sci. USA *95*, 1102–1107.

Moore, T., and Haig, D. (1991). Genomic imprinting in mammalian development: a parental tug-of-war. Trends Genet. *7*, 45–49.

Morison, I.M., Ramsay, J.P., and Spencer, H.G. (2005). A census of mammalian imprinting. Trends Genet. *21*, 457–465.

Morris, T.J., Butcher, L.M., Feber, A., Teschendorff, A.E., Chakravarthy, A.R., Wojdacz, T.K., and Beck, S. (2014). ChAMP: 450k chip analysis methylation pipeline. Bioinformatics *30*, 428–430.

Nagy, A., Sass, M., and Markkula, M. (1989). Systematic non-uniform distribution of parthenogenetic cells in adult mouse chimaeras. Development *106*, 321–324.

Palermo, G.D., Neri, Q.V., Takeuchi, T., and Rosenwaks, Z. (2009). ICSI: where we have been and where we are going. Semin. Reprod. Med. *27*, 191–201.

Pastor, W.A., Chen, D., Liu, W., Kim, R., Sahakyan, A., Lukianchikov, A., Plath, K., Jacobsen, S.E., and Clark, A.T. (2016). Naive human pluripotent cells feature a methylation landscape devoid of blastocyst or germline memory. Cell Stem Cell *18*, 323–329.

Paull, D., Emmanuele, V., Weiss, K.A., Treff, N., Stewart, L., Hua, H., Zimmer, M., Kahler, D.J., Goland, R.S., Noggle, S.A., et al. (2013). Nuclear genome transfer in human oocytes eliminates mitochondrial DNA variants. Nature *493*, 632–637.

Peters, J. (2014). The role of genomic imprinting in biology and disease: an expanding view. Nat. Rev. Genet. *15*, 517–530.

Ran, F.A., Hsu, P.D., Wright, J., Agarwala, V., Scott, D.A., and Zhang, F. (2013). Genome engineering using the CRISPR-Cas9 system. Nat. Protoc. *8*, 2281–2308.

Reik, W., and Walter, J. (2001). Genomic imprinting: parental influence on the genome. Nat. Rev. Genet. *2*, 21–32.

Revazova, E.S., Turovets, N.A., Kochetkova, O.D., Kindarova, L.B., Kuzmichev, L.N., Janus, J.D., and Pryzhkova, M.V. (2007). Patient-specific stem cell lines derived from human parthenogenetic blastocysts. Cloning Stem Cells *9*, 432–449.

Rugg-Gunn, P.J., Ferguson-Smith, A.C., and Pedersen, R.A. (2005). Epigenetic status of human embryonic stem cells. Nat. Genet. *37*, 585–587.

Rugg-Gunn, P.J., Ferguson-Smith, A.C., and Pedersen, R.A. (2007). Status of genomic imprinting in human embryonic stem cells as revealed by a large cohort of independently derived and maintained lines. Hum. Mol. Genet. *16 Spec No. 2*, R243–R251.

Sagi, I., Chia, G., Golan-Lev, T., Peretz, M., Weissbein, U., Sui, L., Sauer, M.V., Yanuka, O., Egli, D., and Benvenisty, N. (2016a). Derivation and differentiation of haploid human embryonic stem cells. Nature *532*, 107–111.

Sagi, I., Egli, D., and Benvenisty, N. (2016b). Identification and propagation of haploid human pluripotent stem cells. Nat. Protoc. *11*, 2274–2286.

Sheaffer, K.L., and Kaestner, K.H. (2012). Transcriptional networks in liver and intestinal development. Cold Spring Harb. Perspect. Biol. *4*, a008284.

Stelzer, Y., Yanuka, O., and Benvenisty, N. (2011). Global analysis of parental imprinting in human parthenogenetic induced pluripotent stem cells. Nat. Struct. Mol. Biol. *18*, 735–741.

Stelzer, Y., Sagi, I., and Benvenisty, N. (2013). Involvement of parental imprinting in the antisense regulation of onco-miR-372-373. Nat. Commun. *4*, 2724.

Stelzer, Y., Bar, S., Bartok, O., Afik, S., Ronen, D., Kadener, S., and Benvenisty, N. (2015). Differentiation of human parthenogenetic pluripotent stem cells reveals multiple tissue- and isoform-specific imprinted transcripts. Cell Rep. *11*, 308–320.

Surani, M.A., and Barton, S.C. (1983). Development of gynogenetic eggs in the mouse: implications for parthenogenetic embryos. Science *222*, 1034–1036.

Surani, M.A., Barton, S.C., and Norris, M.L. (1984). Development of reconstituted mouse eggs suggests imprinting of the genome during gametogenesis. Nature *308*, 548–550.

Surani, M.A., Barton, S.C., and Norris, M.L. (1986). Nuclear transplantation in the mouse: heritable differences between parental genomes after activation of the embryonic genome. Cell *45*, 127–136.

Teramura, T., Onodera, Y., Murakami, H., Ito, S., Mihara, T., Takehara, T., Kato, H., Mitani, T., Anzai, M., Matsumoto, K., et al. (2009). Mouse androgenetic embryonic stem cells differentiated to multiple cell lineages in three embryonic germ layers in vitro. J. Reprod. Dev. *55*, 283–292.

Theunissen, T.W., Friedli, M., He, Y., Planet, E., O'Neil, R.C., Markoulaki, S., Pontis, J., Wang, H., Iouranova, A., Imbeault, M., et al. (2016). Molecular Criteria for Defining the Naive Human Pluripotent State. Cell Stem Cell *19*, 502–515.

Thomson, J.A., Itskovitz-Eldor, J., Shapiro, S.S., Waknitz, M.A., Swiergiel, J.J., Marshall, V.S., and Jones, J.M. (1998). Embryonic stem cell lines derived from human blastocysts. Science *282*, 1145–1147.

Trapnell, C., Williams, B.A., Pertea, G., Mortazavi, A., Kwan, G., van Baren, M.J., Salzberg, S.L., Wold, B.J., and Pachter, L. (2010). Transcript assembly and quantification by RNA-Seq reveals unannotated transcripts and isoform switching during cell differentiation. Nat. Biotechnol. *28*, 511–515.

Tucci, V., Isles, A.R., Kelsey, G., and Ferguson-Smith, A.C.; Erice Imprinting Group (2019). Genomic imprinting and physiological processes in mammals. Cell *176*, 952–965.

Uhlén, M., Fagerberg, L., Hallström, B.M., Lindskog, C., Oksvold, P., Mardinoglu, A., Sivertsson, Å., Kampf, C., Sjöstedt, E., Asplund, A., et al. (2015). Proteomics. Tissue-based map of the human proteome. Science *347*, 1260419.

Weksberg, R., Shuman, C., and Beckwith, J.B. (2010). Beckwith-Wiedemann syndrome. Eur. J. Hum. Genet. *18*, 8–14.

Xu, R.-H., Chen, X., Li, D.S., Li, R., Addicks, G.C., Glennon, C., Zwaka, T.P., and Thomson, J.A. (2002). BMP4 initiates human embryonic stem cell differentiation to trophoblast. Nat. Biotechnol. *20*, 1261–1264.

Yamada, M., Johannesson, B., Sagi, I., Burnett, L.C., Kort, D.H., Prosser, R.W., Paull, D., Nestor, M.W., Freeby, M., Greenberg, E., et al. (2014). Human oocytes reprogram adult somatic nuclei of a type 1 diabetic to diploid pluripotent stem cells. Nature *510*, 533–536.

STAR★METHODS

KEY RESOURCES TABLE

REAGENT or RESOURCE	SOURCE	IDENTIFIER
Antibodies		
Rabbit anti-OCT4	Santa Cruz Biotechnology	Cat# sc-9081; RRID:AB_2167703
Rabbit anti-NANOG	Santa Cruz Biotechnology	Cat# sc-33759; RRID:AB_2150401
Mouse anti-TRA-1-60	Santa Cruz Biotechnology	Cat# sc-21705; RRID:AB_628385
Rabbit anti-AFP	Cell Marque	Cat# 203A-16; RRID:AB_1160815
Goat anti-albumin	ICL	Cat# GAL-80A
Donkey-anti-rabbit IgG H&L (Alexa Fluor® 594)	Abcam	Cat# ab150064; RRID:AB_2734146
Donkey-anti-mouse IgG H&L (Alexa Fluor® 594)	Abcam	Cat# ab150112
Donkey-anti rabbit IgG H&L (Cy2)	Jackson ImmunoResearch	Cat# 711-225-152; RRID:AB_2340612
Donkey-anti-goat IgG H&L (Cy5)	Jackson ImmunoResearch	Cat# 705-175-147; RRID:AB_2340415
Bacterial and Virus Strains		
DH5α (*Escherichia coli*)	N/A	N/A
Biological Samples		
Human oocytes	This study	N/A
Human sperm	This study	N/A
Chemicals, Peptides, and Recombinant Proteins		
Knockout Dulbecco's Modified Eagle's Medium (Knockout DMEM)	Thermo Fisher Scientific	Cat# 10829018
Gelatin	MP Biomedicals	Cat# 960317
Knockout Serum Replacement (KSR)	Thermo Fisher Scientific	Cat# 10828028
L-Glutamine	Biological Industries	Cat# 03-020-1A
Nonessential amino acids	Biological Industries	Cat# 01-340-1B
Penicillin and streptomycin	Biological Industries	Cat# 03-031-1B
β-mercaptoethanol	Thermo Fisher Scientific	Cat# 21985023
Human basic fibroblast growth factor (bFGF)	PeproTech	Cat# AF-100-18B
Trypsin–EDTA	Biological Industries	Cat# 03-052-1A
Y-27632	ApexBio	Cat# A3008
mTeSR1 medium	STEMCELL Technologies	Cat# 05850
Matrigel	Corning	Cat# 356231
Ganirelix acetate	Merck-Serono	NDC 0052-0301-51
Gonal-f (recombinant follicle-stimulating hormone)	Merck-Serono	NDC 44087-1117-1
Menopur (human menopausal gonadotropin, hMG)	Ferring Pharmaceuticals	NDC 55566-7501
Ovitrelle (human chorionic gonadotropin, hCG)	Merck-Serono	NDC 44087-1150-1
Lupron (leuprolide acetate)	AbbVie	NDC 0781-3006-42
Cumulase	CooperSurgical	Cat# 16125000
Global total medium	Life Global	Cat# LGGT-100
ISolate – Sperm separation medium	Irvine Scientific	Cat# 99264
Quinn's Sperm Washing Medium (QSWN)	Origio	Cat# ART-1006
Freezing medium TYB with glycerol & gentamycin	Irvine Scientific	Cat# 90128
G-MOPS Plus medium	Vitrolife	Cat# 10130
Global Total with HEPES	Life Global	Cat# LGTH-050
10% Polyvinylpyrrolidone (PVP) solution with HSA	Irvine Scientific	Cat# 90123
Oil for embryo culture	Irvine Scientific	Cat# 9305
Cytochalasin B	Sigma-Aldrich	Cat# C2743
Fetal bovine serum (FBS)	Thermo Fisher Scientific	Cat# 16000044

(*Continued on next page*)

Continued

REAGENT or RESOURCE	SOURCE	IDENTIFIER
Stemfit medium	Ajinomoto	Cat# ASB01
Geltrex	Thermo Fisher Scientific	Cat# A1413302
TrypLE Express	Thermo Fisher Scientific	Cat# 12604013
Colcemid solution	Biological Industries	Cat# 12-004-1
KCl	Sigma-Aldrich	Cat# P9333
Sodium citrate	Sigma-Aldrich	Cat# W302600
Methanol	Sigma-Aldrich	Cat# 34860
Acetic acid	Sigma-Aldrich	Cat# 320099
Earle's Balanced Salt Solution (EBSS)	Biological Industries	Cat# 02-010-1A
Trypsin–EDTA, no phenol red	Thermo Fisher Scientific	Cat# 15400054
Giemsa stain	Sigma-Aldrich	Cat# GS500
Buffer tablets, pH 6.8	Merck Millipore	Cat# 111374
DPBS	Sigma-Aldrich	Cat# D8662
Formaldehyde 4%	Bio-Lab	Cat# 064503
Triton X-100	Sigma-Aldrich	Cat# T8787
Bovine serum albumin (BSA)	Amresco	Cat# 0332
Hoechst 33258	Sigma-Aldrich	Cat# B2883
O.C.T.	Sakura	Cat# 4583
Hematoxylin solution	Sigma-Aldrich	Cat# GHS316
Eosin Y solution	Sigma-Aldrich	Cat# HT110316
5-Aza-2′-deoxycytidine (decitabine)	Cayman Chemicals	Cat# 11166
TrypLE Select	Thermo Fisher Scientific	Cat# 12563029
Human BMP4	PeproTech	Cat# 120-05
RPMI 1640 medium	Thermo Fisher Scientific	Cat# 21875034
B-27 supplement	Thermo Fisher Scientific	Cat# 17504044
Activin A	PeproTech	Cat# 120-14E
Murine WNT3A	PeproTech	Cat# 315-20
Human HGF	PeproTech	Cat# 100-39H
DMSO	Sigma-Aldrich	Cat# D4540
Iscove's Modified Dulbecco's Media (IMDM)	Sigma-Aldrich	Cat# I3390
Insulin-transferrin-selenium (ITS) solution	Thermo Fisher Scientific	Cat# 41400045
Dexamethasone	Sigma-Aldrich	Cat# D4902
Human oncostatin M	PeproTech	Cat# 300-10
Lipofectamine 2000 Transfection Reagent	Thermo Fisher Scientific	Cat# 11668027
Critical Commercial Assays		
MycoAlert *Mycoplasma* detection kit	Lonza	Cat# LT07-418
Vitrification medium	Kitazato	Cat# VT601US
Leukocyte Alkaline Phosphatase Kit	Sigma-Aldrich	Cat# 86R
TruSeq RNA Library Prep Kit	Illumina	Cat# RS-122-2001
gSYNC DNA Extraction Kit	Geneaid	Cat# GS100
NucleoSpin RNA Plus Kit	Macherey-Nagel	Cat# 740984
qScript cDNA Synthesis Kit	Quantabio	Cat# 95047
GenElute Mammalian Genomic DNA Miniprep Kit	Sigma-Aldrich	Cat# G1N350
EZ DNA Methylation-Direct Kit	Zymo Research	Cat# D5020
FastStart Taq DNA polymerase	Sigma-Aldrich	Cat# 4738314001
PerfeCTa SYBR Green FastMix	Quantabio	Cat# 95072
GoTaq Green Master Mix	Promega	Cat# M7122

(*Continued on next page*)

Continued

REAGENT or RESOURCE	SOURCE	IDENTIFIER
Deposited Data		
RNA-seq datasets, see Table S4	This study	GEO: GSE114679
DNA methylation array datasets, see Table S5	This study	GEO: GSE114679
Experimental Models: Cell Lines		
Human androgenetic ESC line aES1	This study	N/A
Human androgenetic ESC line aES3	This study	N/A
Human androgenetic ESC line aES5	This study	N/A
Human androgenetic ESC line aES7	This study	N/A
Human androgenetic ESC line aES8	This study	N/A
Human androgenetic ESC line aES9	This study	N/A
Human parthenogenetic ESC line pES6	Paull et al., 2013	N/A
Human parthenogenetic ESC line pES7	Paull et al., 2013	N/A
Human parthenogenetic ESC line pES10	Sagi et al., 2016a	N/A
Human parthenogenetic ESC line pES12	Sagi et al., 2016a	N/A
Human IVF ESC line CU-ES4	This study	N/A
Human IVF ESC line CU-ES5	This study	N/A
Human IVF ESC line HuES14	Chen et al., 2009	RRID:CVCL_B144
Human IVF ESC line NYSCF2	Sagi et al., 2016a	RRID:CVCL_AX70
Human IVF ESC line WA09	Thomson et al., 1998	RRID:CVCL_9773
IGF2-KO aES1 cell line	This study	N/A
IGF2-KO aES3 cell line	This study	N/A
Experimental Models: Organisms/Strains		
NOD-SCID *Il2rg*$^{-/-}$ mice	Jackson Laboratory	N/A
Oligonucleotides		
See Table S8		
Recombinant DNA		
pGEM-T vector	Promega	Cat# A3600
pSpCas9(BB)-2A-GFP (PX458)	Addgene	#48138
Software and Algorithms		
CellProfiler (v3.1.5)	Carpenter et al., 2006	N/A
R	https://www.r-project.org	N/A
STAR (version 2.5)	Dobin et al., 2013	N/A
HTSeq (version 0.6.1p1)	Anders et al., 2015	N/A
DESeq2 (version 1.14.1)	Love et al., 2014	N/A
Tophat2 (version 2.0.8b)	Kim et al., 2013	N/A
Cufflinks (version 2.2.1)	Trapnell et al., 2010	N/A
Burrows-Wheeler Aligner (BWA)	Li and Durbin, 2009	N/A
GATK HaplotypeCaller (version 3.2.2)	McKenna et al., 2010	N/A
ChAMP (version 2.4.0)	Morris et al., 2014	N/A
DAVID (version 6.8)	Huang et al., 2009	N/A
Zhang lab sgRNA design online tool	Ran et al., 2013	N/A
Other		
35 mm glass bottom dish	MatTek	Cat# P35GCol-1.5-10-C
ICSI micropipette	Origio	Cat# MIC-SI-20
Humagen micropipette PIEZO-(20)-15, 20 μm inner diameter, 15° angled	Origio	Cat# PIEZO-20-15
Oosight Imaging System	Hamilton Thorne	N/A
Lykos laser	Hamilton Thorne	N/A

(*Continued on next page*)

Continued

REAGENT or RESOURCE	SOURCE	IDENTIFIER
Narishige micromanipulator	Narishige	N/A
Heated Stage	Tokai Hit	N/A
Heracell 150i tri-gas incubator	Thermo Fisher Scientific	N/A
Illumina HiSeq 2500	Illumina	N/A
Illumina NextSeq 500	Illumina	N/A
ABI PRISM 3730xl DNA Analyzer	Applied Biosystems	N/A
7300 Real-Time PCR System	Applied Biosystems	N/A
Inverted Microscope	Olympus IX73	N/A
BD FACSAria III	BD Biosciences	N/A

LEAD CONTACT AND MATERIALS AVAILABILITY

Further information and requests for resources and reagents should be directed to and will be fulfilled by the Lead Contact, Nissim Benvenisty (nissimb@mail.huji.ac.il).

EXPERIMENTAL MODEL AND SUBJECT DETAILS

Human subjects

All research involving human subjects was reviewed and approved by the Columbia University Medical Center IRB under protocol AAAI1347. Anonymous oocyte donors and sperm donors provided written informed consent. All samples were labeled with a number or letter, and were de-identified.

Animals

NOD-SCID *Il2rg*$^{-/-}$ immunodeficient mice (Jackson Laboratory) were used for teratoma formation assays. Mice were handled in accordance with institutional guidelines. Experimental procedures were approved by the institutional ethics committee of the Hebrew University.

Cell lines

Human ESC lines used in this study included six newly-derived aESC lines (aES1, aES3, aES5, aES7, aES8, aES9) (see below), four formerly-derived pESC lines (pES6, pES7 (Paull et al., 2013), pES10, pES12 (Sagi et al., 2016a)), and five human ESC lines derived following IVF (CU-ES4, CU-ES5 (see below), HuES14 (Chen et al., 2009), NYSCF2 (Sagi et al., 2016a) and WA09 (Thomson et al., 1998)). *IGF2*-KO cell lines were generated from aES1 and aES3 cells as described below. For routine culturing, human ESCs were grown on mitomycin-arrested mouse embryonic fibroblasts (MEFs) in 0.2% gelatin-coated plates, in human ESC medium consisting of Knockout DMEM (Thermo Fisher Scientific) supplemented with 15% KSR (Thermo Fisher Scientific), 2 mM L-glutamine (Biological Industries), 0.1 mM nonessential amino acids (Biological Industries), penicillin and streptomycin (50 units ml^{-1} and 50 μg ml^{-1}, respectively; Biological Industries), 0.1 mM β-mercaptoethanol (Thermo Fisher Scientific) and 8 ng ml^{-1} human bFGF (PeproTech). Once ESC colonies reached 80–90% confluence, the cells were passaged by dissociation into small clusters using Trypsin–EDTA (Biological Industries) and replating on new MEF-containing plates, with 10 μM ROCK inhibitor Y-27632 (ApexBio) added to the medium for 1 day after passaging. Prior to directed differentiation assays, human ESCs were cultured in mTeSR1 medium (STEMCELL Technologies) on Matrigel-coated plates (Corning). The cells were maintained in a humidified incubator at 37°C and 5% CO_2 and were free of *Mycoplasma* (testing using MycoAlert *Mycoplasma* detection kit, Lonza).

METHOD DETAILS

Oocyte donation

Female donors underwent controlled ovarian stimulation (COS), where gonadotropin-releasing hormone (GnRH) antagonist ganirelix acetate (Merck-Serono) was given daily from day 6 of COS until the day ovulation was triggered. Gonadotropins were started on day 3 of menstruation by using recombinant follicle-stimulating hormone Gonal-f (Merck-Serono) combined with hMG (Menopur, Ferring Pharmaceuticals) at a total dose range of 150–225 IU/day, depending on the woman's age, basal hormone assessment, anti-mullerian hormone (AMH) levels, ultrasonographic ovarian antral follicle count and BMI. Monitoring of ovarian response was commenced on day 5 of COS by serial transvaginal ultrasonographic assessments and serum estradiol (E2) levels every 48 h. Final oocyte maturation was triggered when at least two leading follicles achieved a maximum mean diameter of at least 18 mm, with simultaneous subcutaneous administration of 1,500 IU hCG (Ovitrelle, Merck-Serono) and 4 mg of the GnRH-agonist Lupron (AbbVie). Transvaginal ultrasound-guided oocyte retrieval was performed under deep sedation 35 h after hCG/Lupron administration. Collected follicles

were stripped of cumulus cells within 1 h of retrieval by an experienced embryologist. Oocytes were cultured for denuding of surrounding cumulus cells in HEPES-buffered medium containing cumulase (CooperSurgical). Oocytes were then transported to the research laboratory in a portable incubator at 37°C. Oocytes used for ICSI were from either fresh or frozen cycles. Vitrification was performed according to the manufacturer's instructions (Kitazato). Vitrified oocytes were temporally stored in liquid nitrogen-vapor tanks until processing for the experiments described below. Thawing was performed according to manufacturer's instructions. One strip at a time was removed from liquid nitrogen and rapidly placed in thawing solution for 1 minute, and washed through a gradient until placed in Global Total medium (Life Global) for 1–2 h in a humidified atmosphere at 37°C and 5% CO_2 before undergoing ICSI. Oocytes confirmed as live were used in subsequent experiments.

Sperm donation and processing

Male donors produced a fresh ejaculate sperm sample into a sterile specimen cup after abstinence for 2–5 days. Semen analysis was performed within 1 h of collection according to the methods described by the World Health Organization (Cooper et al., 2010) using a 20 μm MicroCell and chamber. Samples meeting all the following criteria were used: semen volume, 1.5 mL or greater; sperm concentration, 15×10^6 ml^{-1}; total motility (PR + NP), 40% or greater; progressive motility (PR), 32% or greater; strict sperm morphology (normal forms), 4% or greater. Commercially prepared density gradients with a high gradient concentration (90%; "lower") and a more diluted concentration (45%–50%; "upper") (ISolate, Irvine Scientific) were used to separate progressively motile sperm from immotile sperm and debris. In brief, approximately 1–2 mL of the gradient labeled "lower" was first pipetted into the bottom of a 15 mL conical centrifuge tube, and an equal volume of the "upper" gradient was added on top. 1–2 mL of semen was then layered on top of the two-layered gradient, followed by centrifugation for 10–20 min at 300 *g*. The supernatant was discarded, and the pellet was transferred with a clean sterile pipette into a conical tube. The pellet was then resuspended in 1–5 mL of QSWM (Origio) and centrifuged for 10 min at 300 *g*, followed by repeated washing as described above. Finally, the pellet was resuspended in a few drops of QSWM for ICSI. All male donors were requested to provide a 'backup sample', which was cryopreserved by a slow-freeze cryopreservation methodology using freezing medium TYB with glycerol & gentamycin (Irvine Scientific). Semen samples underwent a time-based freezing protocol using the following temperature time sets: temperature decay was held from –1°C per min to –7°C for a total of 28 min; for manual seeding the temperature was held at –7°C for 10 min; from –7°C per min to –30°C for 22 min; and from –30°C per min to –150°C for 2 h. Cryovial samples were then temporally stored into liquid nitrogen in a storage tank in a labeled sleeve. All samples were thawed as follows. First, cryovials containing sperm samples were removed from the cane in the cryocontainer and contents were allowed to thaw at 38–40°C for no more than 10 min. Once thawed, the contents of the vial were transferred into a labeled sterile conical tube for processing as described above, and the entire semen sample was slowly mixed with complete sperm preparation medium. Semen analysis was performed as described above.

In vitro androgenesis

ICSI was performed using standard methods by highly experienced embryologists, as follows. A sterile glass-bottom dish (Matek) was prepared with drops of G-MOPS Plus and one drop of 7% PVP covered by mineral oil, and used from this point forward to cover all media used. Sperm were placed in the 7% PVP solution. Individual moving sperm were selected and sperm tails were inactivated using a needle strike. Individual sperm were aspirated tail first and placed at the tip of a beveled ICSI micropipette (Origio). The plasma membrane of the oocyte was ruptured using aspiration, and sperm heads were placed near the 8 o'clock position of the oocyte. After injection, oocytes were cultured for 3 h in Global Total medium (Life Global). The maternal genome was removed from 3 to 3.5 h post ICSI, during extrusion of the second polar body. This extrusion causes a bulge visible under contrast microscopy, which can be readily removed with a micropipette (Origio) in the presence of 5 $\mu g\ ml^{-1}$ cytochalasin B (Sigma-Aldrich). At the time of removal, abscission does not yet occur and both sets of segregating maternal chromosomes are attached to the anaphase spindle (Figure 1B). An Oosight Imaging System (Hamilton Thorne) was used to confirm proper removal. Detachment of the maternal nuclear DNA from the spindle occurs at ~4 h after ICSI, and removal of the spindle at that time may result in retention of the oocyte genome. Pronucleus formation was assessed at 4 and 16–18 h post ICSI. Eggs were then grown in Global Total medium at 37°C in a humidified atmosphere of 5% CO_2 until day 6 after ICSI. Medium was replaced on day 3 after ICSI. Embryo cleavage and development were recorded every 24–48 h.

Derivation of human ESC lines

Human ESC lines were derived following established procedures (Yamada et al., 2014). In brief, blastocyst trophectoderm was ablated with 400 μs laser pulses (Lykos, Hamilton Thorne) at 100% intensity using 20–30 pulses and avoiding the inner cell mass. Blastocysts with lysed trophectoderm cells were plated on MEF feeder layers prepared 12–24h earlier in KSR-based human ESC medium (see "Cell lines") supplemented with 2.5% FBS and 10 μM Y-27632. aES1 was derived in Stemfit medium (Ajinomoto) supplemented with 10 μM Y-27632 on geltrex (Thermo Fisher Scientific). Human pESCs were obtained by unfertilized oocyte activation (rather than by paternal-genome removal following ICSI), as fertilization is not required for deriving pESCs with a proper maternal imprinting signature, and generating a potentially viable embryo for experimental purposes is unnecessary in the case of pESCs. Routine passaging was performed in KSR-based human ESC medium or Stemfit medium. Depending on the cell line, enzymatic splitting was performed using TrypLE Express (Thermo Fisher Scientific) at a ratio of 1:10 to 1:20.

Short tandem repeat analysis

Short tandem repeat (STR) analysis was performed by Cell Line Genetics on extracted genomic DNA resuspended in water. PowerPlex 16 System was utilized for co-amplification and three-color detection of 15 STR loci and Amelogenin was analyzed by electropherogram. Each cell line was compared with donor STR profiles to establish genetic origins.

Karyotype analysis

Karyotyping by metaphase spread analysis was carried out using the standard G-banding method according to the International System for Human Cytogenetic Nomenclature (ISCN). For mitotic arrest, cells were incubated at 37°C and 5% CO_2 in medium containing 100 ng ml^{-1} colcemid (Biological Industries) for 40 min. Subsequently, the cells were trypsinized, centrifuged at 1,000 rpm at room temperature and resuspended in warm (37°C) hypotonic solution (2.8 mg ml^{-1} KCl and 2.5 mg ml^{-1} sodium citrate), followed by incubation at 37°C for 20 min. The cells were then incubated in fixative solution (3:1 methanol:acetic acid) at room temperature for 5 min, and fixation was repeated three times following centrifugation and resuspension in fixative solution. Cell suspensions were spread on glass slides, which were then placed on a hot plate (60°C) in a humid environment for 2 min, and incubated in a drying oven at 60°C overnight. On the following day, staining was performed by placing the slides into the following solutions at 37°C: EBSS (Biological Industries) (1 min), 1:55 trypsin–EDTA without phenol red (Thermo Fisher Scientific):EBSS (20 s), 1:4 FBS:EBSS (1 min), EBSS (1 min), 2:50 Giemsa stain (Sigma-Aldrich):pH 6.8 buffer (Merck Millipore) (140 s), and pH 6.8 buffer (1 min). For a detailed protocol, see Sagi et al. (2016b).

Immunofluorescence and alkaline phosphatase staining

For immunofluorescence staining, cells were washed with DPBS (Sigma-Aldrich), fixed in 4% formaldehyde (Bio-Lab) for 10 min, and permeabilized and blocked in blocking solution consisting of 0.1% Triton X-100 (Sigma-Aldrich) and either 3% BSA (Amresco) (for OCT4, NANOG and TRA-1-60 staining) or 1% BSA (for AFP and albumin staining) in DPBS. Incubation with primary antibodies (diluted 1:100, except anti-TRA-1-60, which was diluted 1:200) was carried out overnight at 4°C or 2 h in room temperature, followed by incubation with a secondary antibody (diluted 1:200) for 1 h at room temperature and with Hoechst 33258 (Sigma-Aldrich, B2883) for 10 min in room temperature for DNA staining. Samples were washed twice with DPBS after fixation and incubation steps, and antibodies were diluted in blocking solution. All antibodies are detailed in STAR Methods. The mean immunofluorescence signal intensity per cell was quantified using CellProfiler (Carpenter et al., 2006). Alkaline phosphatase staining was performed using Leukocyte Alkaline Phosphatase Kit (Sigma-Aldrich, 86R).

Teratoma formation assay

Approximately 1–2 × 10^6 undifferentiated human ESCs suspended in 100 μL human ESC medium and 100 μL Matrigel (Corning) were injected subcutaneously into NOD-SCID *Il2rg*$^{-/-}$ immunodeficient mice (Jackson Laboratory). Resulting teratomas were dissected and subjected to histological analysis by hematoxylin and eosin staining (O.C.T. cryopreservation, 10-μm sections). RNA extraction for RNA-seq analysis was performed by homogenization of multiple teratoma pieces of approximately 0.5 × 0.5 × 0.5 cm^3, which is considered representative based on the presence of multiple differentiated cell types observed by histological analysis.

RNA sequencing

A complete list of samples analyzed by RNA-seq is detailed in Table S4. For samples from this study, poly(A)$^+$ RNA-seq libraries (RNA integrity number (RIN) > 8) were prepared using Illumina TruSeq RNA Library Prep Kit according to the manufacturer's protocol and sequenced using Illumina HiSeq 2500 or NextSeq 500. Sequencing reads were aligned to the human reference genome (GRCh38/hg38) using STAR (version 2.5) allowing up to 3 mismatches. Gene expression levels were calculated as normalized read counts using HTSeq (version 0.6.1p1) and DESeq2 (version 1.14.1) and analyzed as regularized logarithm (rlog) values. To calculate reads per kilobase per million fragments mapped (RPKM) values, reads were aligned using Tophat2 (version 2.0.8b) followed by quantification with Cuffquant and normalization with Cuffnorm (Cufflinks version 2.2.1).

Expression analysis of known imprinted genes

For analysis of known imprinted genes, a list of known imprinted genes was assembled based on the Catalogue of Imprinted Genes (Morison et al., 2005) (https://www.otago.ac.nz/IGC) and (Bar et al., 2017). Genes were classified as either (1) imprinted, non isoform-specific, (2) imprinted, tissue- or isoform-specific, or (3) having provisional evidence for imprinting (see Table S3). Only genes with average RPKM > 0.05 in bi-parental ESCs were included in the analysis, and genes from classes (2) and (3) were included if they showed expected differential expression patterns according to parent-of-origin (for MEGs, (pESCs/bi-parental ESCs) > 1 and (aESCs/bi-parental ESCs) < 1; and for PEGs, (aESCs/bi-parental ESCs) > 1 and (pESCs/bi-parental ESCs) < 1). See replicates in Table S4.

Expression analysis of previously undescribed imprinted genes

To identify imprinted gene candidates, autosomal genes with average RPKM > 0.05 in bi-parental ESCs and significant differential expression between aESCs and pESCs (FDR < 0.05, determined using DESeq2 (version 1.14.1)) were considered either putative MEGs if they showed an expression ratio (aESCs/bi-parental ESCs) < 0.5, or putative PEGs if they showed an expression ratio (pESCs/bi-parental ESCs) < 0.5. For analysis of allele-specific gene expression, heterozygous SNPs within putative imprinted genes

were extracted from WGS of WA09 cells (Sequence Read Archive (SRA) accession number SRX347299) by alignment of sequencing reads to the GRCh37/hg19 reference genome using Burrows-Wheeler Aligner (BWA), processing using Picard tools (version 1.119) and SNP calling using GATK HaplotypeCaller (version 3.2.2) (Bar et al., 2017). Heterozygosity was determined by an allelic ratio (proportion of reference-allele reads of the total number of reads) of 0.3–0.7 ($n \geq 15$ reads). RNA-seq nucleotide frequencies at heterozygous SNPs were quantified in a pool of 40 datasets of WA09 cells (Table S7) by alignment with STAR (version 2.5) and SNP extraction as with WGS data. Monoallelic expression was defined by an allelic ratio greater than 0.9 ($n > 40$ reads). For direct Sanger sequencing of *S100A14*, gDNA was isolated from WA09 cells using gSYNC DNA Extraction Kit (Geneaid, GS100) and RNA was extracted using NucleoSpin RNA Plus Kit (Macherey-Nagel, 740984) and reverse-transcribed to cDNA using qScript cDNA Synthesis Kit (Quantabio, 95047). SNP-containing sequences were amplified and sequenced using ABI PRISM 3730xl DNA Analyzer (Applied Biosystems) with the primers detailed in Table S8.

Global DNA methylation analysis

Genome-wide analysis of DNA methylation using Infinium HumanMethylation450 BeadChips (Illumina) was performed according to the Infinium HD Methylation Protocol. A complete list of samples is detailed in Table S5. For samples from this study, gDNA was isolated from cell pellets or tumor slices using GenElute Mammalian Genomic DNA Miniprep Kit (Sigma-Aldrich). Data analysis was carried out using the R package *ChAMP* (version 2.4.0). CpG probes with detection p value > 0.01 in at least one sample or bead count < 3 in at least 5% of samples, and probes containing SNPs or mapping to multiple genomic loci were discarded, and remaining probes were normalized with subset-quantile within array normalization (SWAN). Known imprinted DMRs analyzed in this study (Court et al., 2014; Johannesson et al., 2014) are listed in Table S3. Whole-genome bisulfite sequencing data across human tissues was obtained from the Roadmap Epigenomics Project (shown in GRCh37/hg19).

Bisulfite sequencing analysis

For direct bisulfite sequencing, bisulfite conversion of gDNA was performed using EZ DNA Methylation-Direct Kit (Zymo Research) according to the manufacturer's protocol, followed by nested PCR using FastStart Taq DNA polymerase (Sigma-Aldrich) with the primers detailed in Table S8 and annealing at the following temperatures (°C): *ZDBF2* DMR outer PCR: 55; *ZDBF2* DMR inner PCR: 58.5; *S100A14* putative DMR outer PCR: 50; *S100A14* putative DMR inner PCR: 60. PCR products were cloned into the pGEM-T vector (Promega, A3600), followed by transformation into DH5α competent cells and sequencing of individual colonies with ABI PRISM 3730xl DNA Analyzer (Applied Biosystems) using T7 promoter primer (see Table S8).

DNA demethylation analysis

DNA demethylation was carried out by 4-day treatment with varying concentrations of 5-aza-2′-deoxycytidine (Cayman Chemicals, 11166) with daily medium changing. RNA was extracted with NucleoSpin RNA Plus Kit (Macherey-Nagel) and reverse-transcribed to cDNA with qScript cDNA Synthesis Kit (Quantabio), and gene expression levels were analyzed with qRT–PCR with PerfeCTa SYBR Green FastMix (Quantabio, 95072) in 7300 Real-Time PCR System (Applied Biosystems) using the primers detailed in Table S8.

Trophoblast differentiation

Directed differentiation into trophoblast cells was based on several protocols (Amita et al., 2013; Marchand et al., 2011; Xu et al., 2002), with modifications as follows. Human ESCs grown in mTeSR1 medium (STEMCELL Technologies) on Matrigel-coated plates (Corning) were dissociated using TrypLE Select (Thermo Fisher Scientific) and replated at a density of 2.5×10^5 cells per one Matrigel-coated well of a 12-well plate in mTeSR1 supplemented with 10 μM Y-27632 (ApexBio). On the next day, the cells were washed with DPBS (Sigma-Aldrich) and switched to MEF-conditioned human ESC medium containing 8 ng ml^{-1} human bFGF (PeproTech) for 1 day, followed by 7 days in MEF-conditioned human ESC medium lacking bFGF and supplemented with 50 ng ml^{-1} human BMP4 (PeproTech), with daily medium changes. RNA extracted from the cells was subsequently subject to RNA-seq analysis.

Hepatic differentiation

Directed differentiation into the hepatic lineage was carried out according to a published protocol with modifications (Avior et al., 2015), as follows. Human ESCs cultured in mTeSR1 medium (STEMCELL Technologies) on Matrigel-coated plates (Corning) were dissociated using TrypLE Select (Thermo Fisher Scientific) and replated at a density of 1.25×10^5 cells per one Matrigel-coated well of a 12-well plate in mTeSR1 supplemented with 10 μM Y-27632 (ApexBio). On the following day, the cells were washed twice with RPMI 1640 medium (Thermo Fisher Scientific) and kept in RPMI 1640 medium containing 1X B-27 supplement (Thermo Fisher Scientific), 100 ng ml^{-1} activin A (PeproTech), 50 ng ml^{-1} murine WNT3A (PeproTech) and 10 ng ml^{-1} human HGF (PeproTech) for 3 days. Subsequently, the cells were washed twice with DPBS (Sigma-Aldrich) and the medium was switched to Knockout DMEM (Thermo Fisher Scientific) supplemented with 15% KSR (Thermo Fisher Scientific), 2 mM L-glutamine (Biological Industries), 0.1 mM nonessential amino acids (Biological Industries), 0.1 mM β-mercaptoethanol (Thermo Fisher Scientific) and %1 DMSO (Sigma-Aldrich) for 4 days. The cells were then washed twice with DPBS and kept in IMDM (Sigma-Aldrich, I3390) with 2 mM L-glutamine, 1X ITS solution (Thermo Fisher Scientific), 0.5 μM dexamethasone (Sigma-Aldrich), 20 ng ml^{-1} human oncostatin M (PeproTech) and 4 ng ml^{-1} bFGF (PeproTech) for 5 days. The cells were then washed twice with DPBS and grown in RPMI 1640 medium containing 1X ITS, 0.5 μM dexamethasone and 10 ng m^{-1} HGF for additional 4 days, at which time point the cells were either

fixed for Immunofluorescence staining or harvested for RNA extraction for RNA-seq analysis. All media contained 100 units ml^{-1} penicillin and 100 μg ml^{-1} streptomycin (Biological Industries, 03-031-1B). Media were changed on a daily basis.

Analyses of tissue-enriched gene expression

RNA-seq data from different human tissues were obtained from The Human Protein Atlas (Uhlén et al., 2015) as transcripts per million (TPM) expression values. Values lower than 0.5 were floored to 0.5. For studying tissue-enriched gene expression in teratomas, genes expressed in bi-parental ESCs-derived teratomas (average DESeq2 rlog > 1) that were most highly expressed in a specific tissue with TPM > 5, were ranked by the ratio of expression in that tissue to the mean expression across all other tissues (ratio > 5), and the top 30 genes enriched in each tissue were further analyzed (Table S6). In Figure 5C, the expression ratios between aESC- and pESC-derived teratomas to bi-parental ESC-derived teratomas for each gene were calculated by the median of inverse-log DESeq2 rlog values (n = 3 in each group, see Table S4 for sample identities). Analyses of placenta- and liver-enriched gene expression in trophoblast differentiation and hepatic differentiation, respectively, included genes upregulated by at least 2-fold during each differentiation in bi-parental ESCs (DESeq2 FDR < 0.05) and overlapping the top 100 enriched genes in placenta or liver across all tissues analyzed (ranked by the expression ratio relative to the mean across all other tissues (> 10), with TPM > 5 in that tissue). Functional annotation enrichment analysis was performed with DAVID (version 6.8) (Huang et al., 2009) using the Benjamini method for determining statistical significance.

Generation and analysis of *IGF2*-knockout aESC lines

A CRISPR-Cas9 sgRNA targeting a constitutively expressed exon of *IGF2* (Figure 7C) (5′–CCCAATGGGGAAGTCGATGC–3′) was designed using the Zhang lab online tool (http://tools.genome-engineering.org) and cloned into pSpCas9(BB)-2A-GFP (PX458) (Addgene #48138) following an established protocol (Ran et al., 2013) (cloning oligos detailed in Table S8). aES1 and aES3 cells (passages 8 and 10, respectively) were incubated for 1 h with 10 μM Y-27632, dissociated with TrypLE Select (Thermo Fisher Scientific), transfected with 25 μg targeting vector DNA using Lipofectamine 2000 Transfection Reagent (Thermo Fisher Scientific) and replated on MEFs in human ESC medium supplemented with 10 μM Y-27632. 48 h post transfection, GFP-positive aESCs were sorted using BD FACSAria III (BD Biosciences) and replated as after transfection. To screen for *IGF2* mutants, multiple subclones were isolated, gDNA was amplified using GoTaq Green Master Mix (Promega, M7122) (see Table S8, annealing at 63°C) and PCR products were cloned into the pGEM-T vector (Promega, A3600) followed by transformation into DH5α competent cells and sequencing of individual colonies with ABI PRISM 3730xl DNA Analyzer (Applied Biosystems). *IGF2* mutations were also confirmed by analysis of RNA-seq reads. Control WT and *IGF2*-KO aESCs were differentiated by hepatic differentiation as described above, and the resulting cells were analyzed by RNA-seq. For differential gene expression analysis, DESeq2 was applied using paired sample testing.

QUANTIFICATION AND STATISTICAL ANALYSIS

Details on quantification and statistical analysis have been explained in the figure legends and the Method Details section. n represents the number of samples and/or replicates included in each analysis. The identity and type of samples and replicates in RNA-seq analysis and DNA methylation analysis are specified in Tables S4 and S5, respectively. R was used to calculate *Z*-scores and correlation coefficients, generate plots, and perform PCA, linear regression and statistical tests.

Mean values in Figures 1G, 4B, 6E, 7A, 7B, S2A, and S4E are displayed with error bars indicating standard error of the mean (SEM). p values in Figure 3C were calculated using a linear regression test. p values in Figures 5B, 5C, 6D, 6E, S4E, and S5B were calculated using two-tailed unpaired Student's t test. Corrected p values in Figure 7D were calculated using the Benjamini method. *Q* values in Figure 7E represent FDR values as determined by DESeq2 using paired sample testing.

RNA-seq samples of undifferentiated ESCs (Figures 1G, 2A, 4A, 4B, 5A, 5B, 6A, 6C, and 6D) include aESCs (n = 6): aES1 (mean of 2 biological replicates), aES3 (mean of 2 biological replicates), aES5 (mean of 2 biological replicates), aES7, aES8 and aES9; pESCs (n = 5): pES2, pES6, pES7, pES10 (mean of 3 biological replicates) and pES12 (mean of 2 biological replicates); and bi-parental ESCs (n = 8): CU-ES4, CU-ES5, CSES7, NYSCF1, NYSCF2, HuES14, HuES53 and HuES64. RNA-seq samples of fibroblasts (n = 2) (Figure 1G) include BJ fibroblasts and 1018 fibroblasts. RNA-seq samples of ESCs following trophoblast differentiation (Figures 5A and 5B) include differentiated aESCs (n = 3): aES1, aES3 and aES5; differentiated pESCs (n = 3): pES6, pES10 and pES12; and differentiated bi-parental ESCs (n = 3): CU-ES4, CU-ES5 and HuES14. RNA-seq samples of ESC-derived teratomas (Figures 5C and 5D) include aESC-derived teratomas (n = 3): aES1 T, aES3 T and aES5 T; pESC-derived teratomas (n = 3): pES10 T, pES12 T1 and pES12 T2; and bi-parental ESC-derived teratomas (n = 3): CU-ES4 T, CSES7 T1 and CSES7 T2. RNA-seq samples of ESCs following hepatic differentiation (Figures 6A, 6C, 6D, 6E, 7A, 7B, and S5C) include differentiated aESCs (n = 3): aES1, aES3 and aES5; differentiated pESCs (n = 3): pES6, pES10 and pES12; and differentiated bi-parental ESCs (n = 3): CU-ES4, CU-ES5 and HuES14. RNA-seq samples of WT and *IGF2*-KO aESCs following hepatic differentiation (Figures 7D–7F) include technical triplicates of each of the following: WT aES1, WT aES3, *IGF2*-KO aES1 and *IGF2*-KO aES3.

DNA methylation samples (Figures 2B and S4D) include sperm samples (n = 3): sperm A, sperm D and sperm F; androgenetic samples (n = 4): aESCs (aES3 and aES5) and aESC-derived teratomas (aES1 T and aES3 T); bi-parental samples (n = 4): bi-parental ESCs (CU-ES4, CU-ES5 and NYSCF1) and bi-parental ESC-derived teratoma (CU-ES4 T); parthenogenetic samples (n = 4): pESCs (pES7, pES10 (mean of 3 biological replicates) and pES12 (mean of 3 biological replicates)) and pESC-derived teratoma (pES10 T). Samples in Figures 2C and S2A also include aESC sample aES1 (n = 5).

Correlation and linear regression analyses (Figures 3, S2C, and S3) include samples for which both RNA-seq and DNA methylation data were obtained (n = 3 for each group): aESCs RNA-seq: aES1 (mean of 2 biological replicates), aES3 (mean of 2 biological replicates) and aES5 (mean of 2 biological replicates); aESCs DNA methylation: aES1, aES3 and aES5; bi-parental ESCs RNA-seq: CU-ES4, CU-ES5 and NYSCF1; bi-parental ESCs DNA methylation: CU-ES4, CU-ES5 and NYSCF; pESCs RNA-seq: pES7, pES10 (mean of 3 biological replicates) and pES12 (mean of 2 biological replicates); pESCs DNA methylation: pES7, pES10 (mean of 3 biological replicates) and pES12 (mean of 2 biological replicates).

Expression values from qRT-PCR (Figure S4E) were obtained from biological triplicates of aESCs at each 5-azadC concentration, bi-parental ESCs and pESCs, using *GAPDH* expression for normalization.

DATA AND CODE AVAILABILITY

RNA-seq and DNA methylation array data have been deposited at the Gene Expression Omnibus under accession number GEO: GSE114679.